CORONAL TRANSPORT OF SOLAR FLARE PARTICLES

J. PEREZ-PERAZA

*Instituto Nacional de Astrofisica, Optica y Electronica, Tonantzintla, A.P. 51, 72000 Puebla, México**

(Received 26 April, 1985; in revised from 14 February, 1986)

Abstract. We reviewed the observational features supporting the view that azimuthal transport of solar flare particles takes place at the level of the solar corona, and not in the interplanetary medium. A brief description is given of models regarding longitudinal particle transport, in terms of their ability to explain the corresponding observational phenomena. Finally, a model with multiple particle emission phases is proposed, in terms of two coronal azimuthal transport steps, on the basis of the dynamical and static features of the coronal magnetic field, respectively.

1. Introduction

It is well known that the study of solar particle transport is not only related to the knowledge of the phenomenon itself, but may apply also in the study of the dynamics of charged particle motion through electromagnetic fields, and in the knowledge of coronal and interplanetary magnetic field configurations.

For studying solar particle transport, we dispose of observational elements that make it possible to locate the site and time of solar particle production, in association with solar flares or specific active centers on the solar disk. We also know the time, the location and their arrival directions when they are detected, either at earth or in spacecraft. What is not subject to direct observation is the behavior between their generations and detection. In fact, all observational characteristics of solar particle events, such as time-intensity profiles, longitudinal distributions, anisotropies, and energy spectra, as seen at the point of observation is a combination of several processes taking place from their production till their detection. However, it is not easy to know exactly the number of processes involved in particle transport, nor the relative role of each one, unless we could perform enough specific observations of different kinds in order to separate the effects of each process involved. We note here that solar particles leaving the source environment need to travel through two different magnetic field topologies, namely those of the corona and interplanetary space. Thus, the earlier works were directed to particle transport through the interplanetary magnetic field, under the assumption of impulsive ejection of particles from the source to the base of the interplanetary magnetic field lines. Therefore, particle profiles, anisotropies, longitudinal distributions, and modulation of the energy spectrum were determined exclusively by interplanetary transport. It is now realized that gradual particle control by coronal magnetic fields may become of fundamental importance in quite a large number of solar

* On leave from the Instituto de Geofisica, UNAM, 04510-CU, México, D.F.

Space Science Reviews **44** (1986) 91–138.

particle events. In particular, there now appears to be an established consensus that the azimuthal distribution of solar particles relative to the flare-observant connecting field line takes place mainly in the corona, not during interplanetary transport.

The aim of this paper is to give a summary of the main advances in connection with the phenomenon of coronal transport of solar particles. Due to the lack of elements for absolute discrimination among different effects it will be designated in an arbitrary form, for coronal transport all those processes involved during coronal particle propagation, in the eventual stages of particle storage, and finally particle escape into interplanetary space.

2. Coronal versus Interplanetary Propagation for Azimuthal Particle Transport

Measurements of magnetic field irregularities allow one to determine the relative size of the parallel $\kappa_{\parallel}$ and perpendicular $\kappa_{\perp}$ diffusion coefficients for particle transport in interplanetary space, however, these measurements are not always confident enough to determine the ratio $(\kappa_{\parallel}/\kappa_{\perp})$, and in addition, there is still some controversy about the validity of the theory employed to calculate the coefficients from magnetic field fluctuations. Nevertheless, it has been concluded from other sources that interplanetary propagation is basically carried out along magnetic field lines, through a diffusive-type transport in interplanetary magnetic field irregularities (e.g., Coleman, 1966), where the transversal diffusion coefficient to the mean interplanetary magnetic field is much smaller in relation to the parallel diffusion coefficient $(\kappa_{\parallel}/\kappa_{\perp} \ll 1)$. This assumption is based on the following features:

(1) Strong anisotropy (50–100%) in the initial phase of solar particle events aligned with the sunobservant field line of connection (e.g., O'Gallagher and Simpson, 1966; Rao *et al.*, 1971). This feature is observed in high-energy protons (Duggal *et al.*, 1971) and in electrons (e.g., Allum *et al.*, 1971). In the case of low-energy protons, anisotropy may last some days, up to the end of events (Krimigis *et al.*, 1971).

(2) In order for solar corrotating events to subsist several rotations (e.g., McDonald and Desai, 1971) it is needed that $\kappa_{\perp} \ll \kappa_{\parallel}$, otherwise the flux would be azimuthally dispersed and lost (McKibben, 1973).

(3) The strong temporal difference between the onset arrival times of particle fluxes observed in different spacecrafts placed very close to each other indicates that transport is performed within *'magnetic flux tubes'*, in a very independent form between adjacent *flux tubes*, implying that the properties of fluxes depend only on the way they were injected into the root of interplanetary field lines (Krimigis *et al.*, 1971).

(4) The aleatory motion of interplanetary field lines (Jopikii and Parker, 1969) is not efficient enough to produce azimuthal dispersion of flare particles, and can only explain small changes in the direction of the anisotropy (Roelof and Krimigis, 1973).

(5) Cross-field diffusion may play only a minor role in transporting particles from one field line to the next in *long-lived-events* (Gold *et al.*, 1977).

On the other hand, there are many solar particle events observed on earth which are

associated with solar flares in all the visible and invisible solar disks. This indicates that very often the acceleration region is very far away from the root of the sun-earth connecting field line located at 60° W (Bukata *et al.*, 1972). So, particles need to undergo considerable azimuthal dispersion to reach the base of those field lines if particles have been seen on earth. Since this propagation in heliolongitude cannot take place in interplanetary space, based on the above arguments, longitudinal shifts must occur before the bulk of particles escape into interplanetary space (where their propagation is basically of unidimensional character in the direction of the magnetic field). Convincing evidence has been provided by Reinhard and Wibberenz (1974) and Roelof (1973) that azimuthal transport of solar particles takes place in the solar corona as opposed to perpendicular diffusion in interplanetary space. Some *inferences* supporting coronal transport before particle escape though *model-dependents* are, however, interesting and should be mentioned:

(1) The observational intensity profiles of low energy particles at 1 AU are reproduced better by theoretical profiles if injection is assumed to be finite in time (like storage or azimuthal propagation in the corona) instead of impulsive liberation into interplanetary space (e.g., Feit, 1973; Gombosi *et al.*, 1979).

(2) Exponential decay of fluxes in the last phases of events may be explained without assuming an escape frontier, or a fast variation with radial distance of the diffusion coefficient, if a temporal profile simulating coronal propagation continuous leakage is superposed on interplanetary propagation (Wibberenz and Reinhard, 1975).

(3) Amata *et al.* (1975) have noted that in some events associated with flares very near the sun-observant field line of connection there is a delay in the arrival of particles, which can be understood if particles are first distributed in the corona and then injected into interplanetary space, instead of impulsive ejection.

(4) By means of the potential approximation, Newkirk (1973) calculated the magnetic field topology of some solar flares whose magnetic fields had already been measured. He then compared the longitudinal extension of the open magnetic field line configurations associated with a certain surface of injection, for those flares that produced particle events, with the extension of the longitude of detection. He found no agreement, but the detection range of longitudes was wider. This argues in favour of coronal azimuthal transport.

(5) A Compton–Getting transformation determining the anisotropy in the co-moving frame observed in spacecraft reveals a long lasting residual anisotropy in the co-moving frame, with protons streaming from the sun. This argues against impulsive ejection in some events (Gold *et al.*, 1975).

Once the existence of a certain amount of solar particle propagation in the solar atmosphere is established, it is necessary to determine the properties of such propagation in order to develop physical models for interpreting observational data. The first observations of longitudinal displacements were carried out without much concern for locating such dispersion. Observations were limited to measuring azimuthal gradients and temporal evolution of events from different heliolongitudes of detection; however the conception of two stages of propagation (coronal and interplanetary) was considered

long ago by Lüst and Simpson (1957) in association with the particle event of 23 February, 1956.

3. Observational Properties of Coronal Propagation

To separate coronal propagation from interplanetary transport and establish the properties of azimuthal transport, observations have been carried out in two different forms:

(1) Observation from one unique point in interplanetary space (the Earth for instance) of several flare particle events taking place at different sites throughout the solar disk.

(2) Observation of individual particle events simultaneously with several spacecrafts located along different heliolongitudes and helioradii (e.g., Kunow *et al.*, 1981; McGuire *et al.*, 1983a; Lockwood and Debrunner, 1984).

The statistical study of these data furnish the most common behavior of particle coronal propagation. It is worth mentioning that the transport of flare particles in the solar corona is not only azimuthal but also radial. However, the kind of information that we can draw from data is not enough to support the characteristics of such a radial propagation. Preliminary work in this direction with multiple spacecraft observations (McGuire *et al.*, 1983a) seems to indicate that the magnitude of any radial effect is small when compared with longitudinal effects. Obviously, the observational information is concerned with the last step of coronal propagation, when particles are liberated. Exactly what happens between the time of acceleration and the time of escape remains masked to direct observations. We can only observe the final effects. Even the data obtained from this last step is not of absolute precision because of the limitations of corrective techniques for interplanetary effects; that is, the time-dependent azimuthal distribution of particles at the time of coronal liberation may, in principle, be deduced from the time-intensity profiles measured along different longitudes at the level of the Earth's orbit, after subtracting the effects of interplanetary propagation. However, in that case, one must make supositions about interplanetary propagation, which condition results on the validity of the adopted model. The most common technique has been the mapping of the measured fluxes back to the Sun, by simple projection of particle intensity along the magnetic field line, connecting the observant with the solar corona. This assumes what we have previously emphasized, that interplanetary propagation is basically along the magnetic field lines. However, here again, it is necessary to adopt a model for the interplanetary magnetic field; generally, the *Extrapolation Quasi-Radial Hyper-Velocity Model* of Notle and Roelof (1973), which accounts for time-dependent solar wind velocities is assumed. The mapping method was first used by Bukata *et al.* (1972); Roelof and Krimigis (1973); Gold *et al.* (1973). In particular, the latter authors were able to isolate spatial and temporal variations. Using multispacecraft observations at four different heliolongitudes, Bukata *et al.* (1972) studied the particle events of March–April 1969 and found that flare particles were detected over the 360° of the heliolongitude with a strong influence of azimuthal gradients on the temporal evolution of fluxes. By mapping the fluxes to the Sun, they were able to locate the flare site of

events which occurred on the hidden hemisphere of the Sun, under the assumption that the point of major emission should concur with the flare position. This, however, is not always true, since it has been observed that in some events, the major intensity of flux is injected from a longitude far from the source flare (Gold *et al.*, 1977). In addition, this mapping technique is valid mainly in the initial phase of events, when particles travel with very few dispersions through the irregularities of the field, in the magnetic flux tubes of their propagation; for later times it is rather valid for very high energy particles, or even low energy particles, if the spacecraft are very near the Sun, as for instances the Helios spacecraft (Kunow *et al.*, 1977), in which case interplanetary propagation plays a minor role. Nevertheless, in spite of the limitations of observational techniques, it has been possible to deduce the following properties of coronal transport:

(a) The onset time of the event and the time of peak intensity increase (or at least remain constant) with the azimuthal separation between the observant and the flare site (Fan *et al.*, 1968; Reinhard and Wibberenz, 1974; Van Hollebeke *et al.*, 1975; Ma Sung *et al.*, 1975; Datlowe, 1975; McKibben, 1972; Simnett, 1971, 1972; Barouch *et al.*, 1971; Sakurai, 1971; Lanzerotti, 1973).

(b) The time-intensity profile widens with the longitudinal separation between the observant and the flare site (e.g., Reinhard and Wibberenz, 1974) while the maximum intensity is greatly reduced (McCracken *et al.*, 1967; McCracken and Rao, 1970; Van Hollebeke *et al.*, 1975).

(c) The azimuthal distribution of flare particles tends toward uniformity for long times during the decay phase of events (e.g., McCracken *et al.*, 1971; McKibben, 1972).

(d) Azimuthal coronal transport occurs at two different rates: a fast propagation process which covers a longitudinal extension of about 60–100° around the flare site in one hour. The so called Fast Propagation Region (FPR) reports an average velocity of $\langle 50^\circ \mathrm{hr}^{-1} \rangle$, and a slower propagation process, outside of the FPR, where transport is performed at a rate of 24–93° day^{-1} (Fan *et al.*, 1968; Duggal and Pomerants, 1973; Reinhard and Wibberenz, 1973, 1974; Ma Sung *et al.*, 1971; Duggal, 1975). Similar results were found by Anderson and Lin (1966) and Lin (1970) in relation with non-relativistic electrons.

(e) On statistical grounds, the azimuthal propagation of low energy particles is both rigidity and energy independent (McKibben, 1972; Lanzerotti, 1973; Reinhard and Wibberenz, 1973; Ma Sung *et al.*, 1975; Roelof *et al.*, 1975; Gold *et al.*, 1977; Perron *et al.*, 1978; Gombosi *et al.*, 1979). A fine structure of azimuthal propagation behavior shows that the travelling time, over a certain longitudinal distance, is slightly velocity-dependent, as $v^{-0.55}$ (Ma Sung, 1977) and practically rigidity-independent, $R^{-0.07}$ (Ma Sung and Earl, 1978). On the other hand, azimuthal transport of high energy protons (> 100 MeV) tends to behave in an energy and rigidity dependent manner (Bazillevskaya and Vashenyuk, 1979, 1981; Kecskemety *et al.*, 1981). There are, however, other results suggesting that coronal transport of low energy particles may show a stronger velocity dependence or even an energy or rigidity behavior, for instance, in association with coronal diffusion coefficients (e.g., Gombosi *et al.*, 1977; Kunow *et al.*, 1981; Lockwood and Debrunner, 1984), or in relation to variations of the spectral index as

a function of longitudinal distance (McCracken *et al.*, 1971; Van Hollebeke *et al.*, 1975; Conlon *et al.*, 1979). Nevertheless, such an eventual behavior might be attributed to the last steps of coronal transport, i.e., particle escape, or propagation out of the FPR. Therefore, what can be drawn from the general consensus is the following:

(1) For observational points connected with field lines near the flare site, where only interplanetary propagation is important, the phenomenon of velocity dispersion is observed ($vt_m \sim 8.3$ AU, where t_m is the time of maximum intensity).

(2) For observational points connected to the Sun far from the flare site vt_m is not constant, but increases with particle velocity.

(f) Azimuthal propagation is controlled, to a certain extent, by the unipolar field sectors of the large-scale photospheric field. Particle fluxes crossing two sectors of opposite polarity are highly modulated: flux intensity decreases and the onset and peak times increase. This has been observed in low-energy particles (Gold *et al.*, 1973; Roelof and Krimigis, 1973; Roelof *et al.*, 1975; Gold and Roelof, 1979; Reinhard, 1975; Kunow *et al.*, 1977; Reinhard *et al.*, 1977), as well as in high-energy particles (Vashenyuk *et al.*, 1977). The frontiers of unipolar sectors seem to be associated with the coronal extension of chromospheric neutral lines or dark filaments of the low corona. Unipolar sectors behave as extended regions of preferential liberation (Reinhard *et al.*, 1977), and determine large azimuthal gradients among them. Van Hollebeke *et al.* (1975) inferred preferred-connection longitudes of $\sim 60°$ in extension, in agreement with the average dimension of chromospheric unipolar regions (McIntosh, 1972).

(g) Besides property (c), the point of peak intensity moves longitudinally to the west, out of the flare site, up to same definite distance (e.g., $\sim 100°$ for the 10 April, 1969 event) where there is no displacement, as if there were (a) localized zone of preferential liberation, or a strong magnetic barrier. In some events, major intensity may be injected at a different longitude than that of the flare site (Keath *et al.*, 1971; Reinhard and Wibberenz, 1973; Gold *et al.*, 1977; Reinhard *et al.*, 1977).

These seven properties are more or less common to most solar flare particle events. Obviously, the first three look like typical properties of diffusive transport, though the time of maximum intensity increases linearly with azimuthal distance, instead of quadratically as is expected from pure diffusion (Reinhard and Wibberenz, 1973). There are, however, other features that seem not to be general properties of coronal transport, but rather peculiar properties of some specific particle events, or there is no consensus because the results are disperse and show no definite tendency.

(h) The spectral index γ of the power low energy spectra at energies higher than ~ 15 MeV increases with azimuthal distance in the initial phase of events (Van Hollebeke *et al.*, 1975; Conlon *et al.*, 1979), whereas in others, γ remains constant (McKibben, 1972; Perron *et al.*, 1978) but it may decrease with longitudinal distance during the decay phase of some events (McCracken *et al.*, 1971). In Figure 1, this property has been schematized. This is a highly controversial point, where the effects of azimuthal displacement are hardly separable from those of coronal particle escape, or even from energy degradation during particle storage, or an eventual participation of continuous acceleration with a spatial and temporal dependent source strength. At any

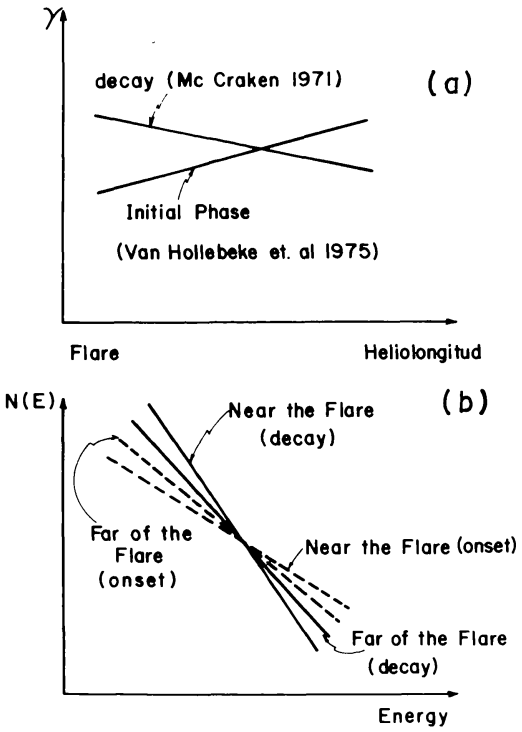

Fig. 1. (a) Spectral slope behavior and (b) Energy spectra behavior according to property (h) of Section 3.

event, this property seems to be ineluctably associated with properties (d), (e), (g) and the diffusive behavior during coronal transport.

(i) McKibben (1972) reported two phases of particle decay in some events where the time-decay constant abruptly increased by a factor of 2–3 from one phase to another. Strong azimuthal gradients were observed in the first phase, and low longitudinal gradients with longer time decay occurred in the second phase. Abrupt transitions were simultaneously observed by two spacecraft widely separated in heliolongitude. Particles of the second component were uniformely distributed in longitude, whereas the first components were rather concentrated over a shorter longitudinal emission extension.

(j) In some events, particle emission lasts longer than the needed time for propagation if particles were simply advancing azimuthally while escaping, and emission may even be prolonged for several days after the flare. Particle storage has been evoked for interpreting this delay (e.g., Simnet and Holt, 1971; Benz and Gold, 1971; Zeldovich *et al.*, 1977; Helios group, 1979). This is supported by radio-waves and X-rays emissions (e.g., Lin, 1970; Simnet, 1971). However, for the survival of low energy particles against collisional losses, a continuous acceleration process must be operating along with particle storage (Krimigis, 1973; Roelof and Krimigis, 1973; McDonald and Desai, 1971).

(k) At least in the particular case of corrotating solar particle events, where a regime of continuous emission is established, the time decay of low-energy particles is longer than for high energy particles. This indicates that azimuthal gradients are higher for low energy particles than for high energy particles (Rao *et al.*, 1971).

Finally, another restriction that should be considered in modelating coronal transport is the occasional occurrence of a preliminary peak in the intensity-time profile of non-relativistic protons before the peak of the bulk of flare particle radiation (personal communication of the GSFC group, 1978). This seems to indicate that particles are impulsively liberated in a nature different than gradual escape.

To conclude the description of the observational points that a suitable model of azimuthal transport of solar flare particles should be able to explain, let me emphasize again that it is not yet possible to categorically determine which are the characteristics of the longitudinal injection profiles that depend on the process of longitudinal propagation, and which depend on the escape mechanism. For instance, azimuthal gradients may be used as indicators of the magnetic field structure, since particle escape is controlled by the magnetic field. The points of major detection of particles indicate that the coronal magnetic field has open field lines in the connection site with the observant, whereas minor particle fluxes should be injected from magnetic structures with closed field lines, where particle escape is more difficult. Alternatively, the site where the flux is weak could have an open field line configuration, but the number of particles arriving at that point may be small due to particular conditions of propagation from the place of production, such as the crossing of a neutral sheet separating two sectors of opposite polarity. Therefore, it is not easy to know if the delay in particle escape or the low-particle intensity in some point is due to the mechanism of propagation, or the mechanism of escape, based on measurement of only the longitudinal distribution of particle fluxes. In fact, as it was already mentioned, by mapping the observational fluxes back to the sun to obtain the longitudinal injection profiles only information on the last step of coronal transport is obtained, while the involved intermediate processes are masked.

4. Modelation of Solar Flare Particle Coronal Transport

With regard to the modelation of coronal transport, models should be able to explain both qualitative and quantitative observational features: on the one hand the models should describe the physical processes involved in coronal transport, and on the other hand give an adequate mathematical description of the effect of these processes on the particle fluxes, so that quantitative predictions can be compared with observations. At present, no model is able to satisfactorily cover both aspects, while giving a global description of the observational features listed in Section 3. Due to a lack of knowledge of all processes taking place from particle production to detection, several proposals for coronal transport have been offered freely in literature. These cannot be definitively approved or disapproved; in fact, observational effects seem not to be of a general nature, but rather change from event to event, and even those properties of a more general character stir quite a bit of controversy among researches. This has led to the development of many models which attempt to explain particle transport of one particular solar event, or a specific kind of peculiar events. However, adequate methodology for understanding solar particle transport may reside in the development

of first, a global description of the physics involved in the overall phenomenon of particle transport, and then, an understanding of the intrinsic peculiarities of specific particle events.

Historically, the first models of coronal transport were developed in a quantitative manner. The basic parameters of each model are derived by solving transport equations and matching them to reproduce the observational time-intensity and anisotropy profiles. The common feature of those models is that they are addressed to giving an account of the shift of onset and maximum intensity times with longitudinal distance, the widening of the profile with azimuthal separation, the trend toward uniformity of longitudinal distributions over a long period of time and the exponential decay of flux intensity in the late phase of particle events. The most basic assumptions usually employed consist of an initial diffusive propagation in the corona, characterized by a diffusion coefficient and an escape time, followed by a second step of diffusion along the interplanetary field lines. Some of these include other effects at the coronal level, such as particle energy losses, collective motions, particle acceleration and disturbances by shock waves and solar wind streams. In fact, those primary models did not take into account modern observations such as the existence of a FPR, and the energy and rigidity-independent nature of the transport process of the major components of solar particles (< 100 MeV) as well as the very slight velocity-dependence of the transport process. On the other hand, most of recent models are rather of a qualitative nature and mainly set out to describe the involved physical processes to explain new observational properties of (d) and (e), and consequently, very often do not generate results of particle fluxes that may be compared with observations.

4.1. Precursor models

Sekido and Murakami (1955) proposed the existence of two different magnetic field configurations where particles are confined. The first was a sphere around the Sun of $\sim 100\ R_\odot$ of radii, where particles were dispersed and then emitted from any point on the sphere surface into the external magnetic field to a weaker but larger extent. In this way, the first stage would distribute particles independently of the flare position. Lüst and Simpson (1957) suggested, in connection with the 23 February, 1956 event, a diffusion region around the Sun ($\sim 30\ R_\odot$), which they called '*the solar envelope*', where there was much more internal diffusion. Once particles escape from the '*envelope*', propagation was 'freer' in a preferential direction determined by the magnetic field line where they left the '*envelope*'. In this way, the authors interpret the strong anisotropy degree of that particular event. In fact, these precursor models which introduce particle propagation around the Sun were not specifically intended to explain azimuthal transport observations

4.2. Models based on transport equations (quantitative results comparable to observational data).

(1) Reid (1964) developed a two dimensional model where flare particles undergo isotropic diffusion in a very narrow layer ($< R_\odot$) before escaping into magnetic flux

tubes of interplanetary space where there is practically no dispersion. This occurs to the extent that the observed time profile of the Earth's orbit represents the number of injected particles from the solar atmosphere without any modification for interplanetary transport. For the 28 September, 1961 event, this model is able to describe the early phase of the event. For a long time, interplanetary propagation played an important role. This model may explain properties (a), (b), (c), and (g), of Section 3.

(2) Axford (1965) complimented Reid's coronal diffusion model with anisotropic interplanetary diffusion of the type proposed by Krimigis (1965) where only propagation parallel to the magnetic field is considered. By adjusting five parameters he is able to produce data similar to Bryant *et al.* (1962). This model is able to reproduce observational properties (a), (b), and (c). The main difference between models (1) and (2) is that the time-evolution of particle intensity is of different nature; in Reid's model, the profile is determined by the change of connection longitudes between the Sun and the observer as the Sun is rotating, whereas in the Axford model, interplanetary diffusion is predominant, with particle gradients taking place in the same flux tube. Although coronal diffusion coefficients do not depend explicitly on particle velocity, a small dependence is introduced by using slightly different values for different energy ranges. These models therefore do not contradict property (e).

(3) Burlaga (1970) quantifies the scenario of Lüst and Simpson (1957) in a unidimensional model where the concentration of dispersion centers is higher nearer the Sun than in interplanetary space. However, since propagation is basically in the radial direction, it does not account for any kind of azimuthal particle motion.

(4) Englade (1971) considered along with particle diffusion, collisional energy losses during particle stay in the corona. Here, an explicit energy dependence of the diffusion coefficient ($\kappa \sim E^q$) and of the escape rate ($\beta \sim E^q$) is assumed. For the late phase of the event, coronal injection profiles are superimposed on diffusive interplanetary transport, including convection and adiabatic deceleration. In the initial phase, impulsive injection is considered. No comparisons are made with observational data of specific events, but this model attempts to reproduce general features of the time profiles, energy spectra and anisotropies observed on the Earth's orbit. Coronal energy losses are considered in attempt to explain the decrease of the spectral index of low energy particles in the initial phase of events which cannot be explained by velocity dispersion. This model explains observational properties (a), (b), and (c), without contradicting the other features. In particular, the energy independence of coronal transport might be imposed by setting $q \approx 0$.

(5) Reinhard and Wibberenz (1973, 1974) and Reinhard and Roelof (1973) developed a two dimensional model for solar particle transport outside of FPR. Based on the fact that the maximum intensity of flare particles is not often observed at the flare site, they deduced a deterministic process (longitudinal drift at a rate of 1–4° hr^{-1}) acting along with a stochastic process (longitudinal diffusion parallel to the solar equator), which is generally observed since time-intensity profiles of eastern hemishere events are much wider than those of western hemisphere events. By assuming impulsive injection through a region of preferential longitudes of release of about 60° in extension, the solution to

the transport equation becomes dependent on two basic parameters: the longitudinal drift time τ_E and a characteristic diffusion time τ_D, that are determined by the onset time and the time of maximum intensity of the coronal injection profiles at the connection longitude with the observer. Analysis of 50 proton events shows that, in average, particle drift dominates diffusion in particle transport. By introducing long-lasting injection (Wibberenz and Reinhard, 1975) with a characteristic escape time τ_L, observation of flare particle events or not that take place far from the connection longitude with the observer can be explained in terms of relative importance of τ_L and τ_E. When τ_L is no longer than τ_E, particle loss is relatively small and peak intensity will move far by coronal drift; whereas when $\tau_E > \tau_L$, the particle loss becomes so important, that no particle observation is expected at observational points far from the flare site. Interplanetary profiles are obtained by convolution with the solution of the model of Krimigis (1965). It has been shown that the exponential decay shape of the time intensity profile is explained by finite energy-independent solar injection. So, this model predicts energy independent coronal transport on the basis of average values of the model parameters ($\tau_E = 0.56$ hr deg^{-1}, $\tau_D = 0.22$ hr deg^{-2}, $\tau_L = 23$ hr). Any velocity dispersion appears from the interplanetary diffusion coefficient ($\kappa \sim v$). Therefore, in addition to explaining the exponential decay of flare particle events, this model is consistent with properties (a), (b), (c), (g), and potentially (e), though it does not consider the slight velocity dependence of low-energy particles and energy dependence of high energy protons. Also, explicit assumptions are not included concerning the transport process in the FPR across the first $\sim 60°$ of longitudinal transport, after which the drift and diffusion processes are considered.

(6) Ng and Gleeson (1976) developed a model for coronal diffusion based on Reid's model (1964) that solves in spherical coordinates for an impulsive injection. As in Reid's model, they consider corrotation of the magnetic flux tubes, where particles are distributed among different flux tubes. This model predicts energy-independent transport of low-energy particles, since the coronal diffusion coefficient and the escape rate are both energy-independent. This leaves open the possibility of a phenomenological incorporation of the FPR in the quantitative description. The coronal injection profile is taken as a frontier condition for a unidimensional interplanetary process, with consideration of corrotation of field lines, convection and adiabatic deceleration. The predicted intensity decay is much slower than in Reid's model which is closer to observational behavior. This model is able to explain features (a), (b), (c), and potentially (d) and (e).

Another derivation of Reid's model (1964) was developed by Kunow *et al.* (1981) which is convoluted with the interplanetary model of Owens (1979). It is able to reproduce properties (a), (b), (c) for low-energy particles though there is a divergence with observational data obtained in the later phase of events.

(7) Bazilevskaya and Vashenyuk (1979, 1981) developed an analysis of the injection function of high energy protons ($\gtrsim 100$ MeV) into interplanetary space on the basis of the following assumptions: flare particles fill an acceleration volume of ~ 60–$80°$ of longitudinal extension, while escaping exponentially into interplanetary space, following

a faster propagation step to the roots of interplanetary field lines than predicted by coronal diffusion. The escape and fast propagation processes are energy dependent. For comparisons with observational time intensity and anisotropy profiles, the exponential injection function is convoluted with the formulation for interplanetary transport of Schulze *et al.* (1977). So the main results of this analysis show that almost the entire coronal transit time of high-energy particles is related to escape, independent of solar longitude from a volume of about the same size of that of the FPR. This suggests a similar situation of low-energy particle transport to the connection longitudes near the flare site, i.e., those particles that are injected without undergoing the slow second step of coronal propagation, but only the fast first step. The difference in situations is that escape of high energy protons shows a definite energy-dependence.

(8) McGuire *et al.* (1983b) developed a model which includes coronal diffusion, exponential escape and initial acceleration of local coronal particles over a finite width $\Phi_0 \approx 10\text{–}30°$, centered about the flare site. The initial distribution is Gaussian of width Φ_0 which broadens with time at a rate depending on the amount of diffusion, and drops in intensity at a rate depending on the *e*-folding escape time. Particle distribution remains Gaussian, as far as the diffusion coefficient and escape time are not functions of longitude. Coronal injections profiles are convoluted with the addition of corrotation effects. The effect of corrotation is translated in assymmetry of the predicted profiles about the flare site, in agreement with observational data. The estimated coronal diffusion coefficients and escape time are energy-independent. This model is able to explain properties (a), (b), (c), and (g).

(9) Lockwood and Debrunner (1983, 1984) studied the 7 May, 1978 flare particle event, by means of a two-dimensional model of coronal transport of a Reid's and Axford's type previously mentioned. Given the high degree of anisotropy of the event, they assumed that the detected profiles within the first hour of the event closely represent solar injections profiles, even at energies as low as 50 MeV, so that by tracing the observed fluxes back to the Sun they describe the coronal particle time profiles. Data from two spacecrafts were employed in this study: one at the Earth's orbit (IMP), whose connecting line to the Sun is longitudinally separated by 15°.7 from the flare site, and the other (Helios) very near the Sun, whose connecting line is separated by the opposite side, 32°, from the flare site.

The fact that the measured fluxes are very different at 15°.7 on one side of the flare than the fluxes at 32° on the other side, leads to the conclusion that the fast propagation region cannot extend more than $\pm 25°$ from the flare. So, only one kind of coronal transport process is considered, characterized by a velocity dependent ($E^{0.5}$) diffusion coefficient between 30 and 350 MeV, and an average constant value of the escape rate. In this way, a velocity-dependent coronal transport is predicted even for low energies. The behavior of these two basic parameters of the model are obtained by fitting the deduced coronal profiles with the calculations. This model is able to explain features (a), (b), and (c).

It is interesting to note that if the FPR for this event would be extended symmetrically $\sim \pm 25°$, the difference between the observed fluxes in Helios and those of IMP could

be interpreted in terms that the particle fluxes seen in Helios as having undergone two steps of coronal propagation, the second one with a slower rate of transport out of the FPR, whereas particles seen at IMP have only undergone propagation within the FPR.

The common feature of these nine prototypes of coronal transport models is that they do not furnish a physical scenario for the phenomenon, and scarcely specify the physical processes and coronal structures that give place to particle diffusion, drift, escape and eventually acceleration. Rather they generally determine the values of the parameters of those processes by adjusting predictions with observational data. *It is currently assumed in Astrophysics that a complete model should include a physical scenario and a mathematical description that suitably reproduces observational features.*

4.3. Coronal transport models based on physical scenarios

Most of the models that attempt to explain physical processes are of a qualitative nature, and are limited to some specific properties of coronal transport. For instance, the first proposed models did not take into account the rigidity and energy-independent behavior of low energy particle transport. Below several models are mentioned:

(1) Fan *et al.*'s (1968) open magnetic field topology model proposed a FPR of 100° of extension for protons of 13–70 MeV associated with an open fan-shaped topology over the active region of the flare, whose field lines are connected to the interplanetary field. Within that extended FPR, particles would undergo such a peculiar anisotropic diffusion process that the onset and peak intensity times are practically independent of flare longitude. According to some observations, Lin (1970) attempted to explain the rapid access of flare electrons to a wide range of longitudes by means of an extended source that may be associated with shock wave acceleration. The region occupied by the shock wave would be surrounded by field lines directly connected to the interplanetary field. This open extended region was denominated the 'open cone of propagation', where impulsive electron events proceed. A similar idea was extended by Wang (1972) in the sense that open field lines should allow for electron escape from a very wide region in longitude. In all those proposals, propagation inside and outside the region of rapid access to the interplanetary medium would be energy-dependent. These models may explain property (d), though before a flare takes place it is more common to find closed magnetic field configurations than open field topologies, which are more often created after the flare by the abrupt heating of solar plasma.

(2) McCracken and Rao's (1970) coronal transport model of prompt events: the studies of solar flare particle events by McCracken and Rao established that azimuthal gradients in delayed events were considerably higher than in prompt events. This led the authors to the assumption that azimuthal transport was less important in delayed than in prompt events.

They developed a diffusion model for prompt events occurring in a thin layer 0.5 $R_\odot$ above the photophere where the magnetic field is commonly highly disturbed by the same flux of magnetohydrodynamic waves that dissipates heat into the corona. So, particles diffuse transversally through the magnetic irregularities induced by the MHD waves. Above that layer magnetic fields are more ordered, azimuthal diffusion becomes

negligible and transport is basically in the radial direction. It may be noted that this model fits the mathematical description of the phenomenon given by Reid (1964) and Axford (1965), however, this kind of particle diffusion is energy and rigidity dependent, though properties (a) to (c) can be explained.

(3) The two emission-phase models of Simnet and McKibben: Simnet (1971, 1972) proposed that flare protons and relativistic electrons are emitted in two components, a prompt and a delayed component. It is assumed in this model that when a flare takes place, the coronal magnetic fields is disturbed by the heated plasma that escapes from the magnetic field influence toward interplanetary space. The irregularities produced from that disturbance may act as scatter centers of the flare accelerated particles. Behind that plasma there is a hydromagnetic shock wave that keeps the accelerated particles behind the shock front, until a height of above 3 $R_\odot$ where particles begin to escape, to give rise to the prompt component. Particles that were produced in the flare after the shock waves have swept the region $\leq 3\ R_\odot$, remain confined in strong magnetic fields of the low corona where they diffuse in a longitudinal direction to reach the external corona and interplanetary medium. This component would produce the delayed events, and may even create in some events a corrotating regime, as is often seen with particles of low energy. To explain the emission of low-energy particles in some events before the bulk of flare particles, Simnet assumed that prior to a flare, there is a population of trapped energetic particles produced in precedent solar flares. So, when a new flare occurs some of them are liberated, and others remain confined within the active region, where they are accelerated by the flare process to very high energies. Among the liberated particles, in some cases, only low-energy electrons would be detected previous to the bulk of flare particles, since the velocity of electrons is higher than that of protons of the same energy, so low-energy protons would mix with main flare particles and arrive at the detection point by the same time. To support his hipothesis, Simnet (1972) points out that the first event following a period of low solar activity does not often present a very high-energy component, because particles previously accelerated were not trapped.

To explain property (i), McKibben (1973) proposed that when particles are accelerated in the flare process, some of them may have direct access to interplanetary space by means of open field lines, and others remain trapped in the magnetic field lines. Those that escape directly represent the first phase component, with a strong azimuthal gradient, since longitudinal distribution is determined by the extension of the region of the open field lines. In this case, decay time is determined by the properties of interplanetary propagation. Particles that remain trapped diffuse around the Sun through a layer of about 0.5 $R_\odot$ in height, with an azimuthal diffusion coefficient 10–20 times larger than the radial diffusion coefficient. This component remains in the corona for about 10 days with a mean characteristic residence time of ~ 40 hr. Since azimuthal gradients are small, there would be an established trend toward uniform longitudinal distribution. Therefore, this model is able to furnish an explanation of properties (c) and (i), whereas Simnet's model is able to explain (i) and (k).

(4) The Fisk and Schatten model of Diffuse Transport by Drifts in Neutral Current

Sheets: Fisk and Schatten (1972) have proposed that the low corona may be populated by neutral current sheets due to strong magnetic field gradients prevailing at the top of the chromospheric spicule network. A neutral current sheet is a narrow region where the field changes polarity very abruptly so that a very steep magnetic field gradient and an electric current along the sheet is established. Particles moving within those kinds of structures undergo a certain drift because of the steep field gradients they feel when they cross through a sheet. Because of the change in polarity, particles suffer a displacement on the order of their gyroradii in the neutral sheet, which is translated into a longitudinal motion with a characteristic drift velocity, depending on the width of the neutral current sheet. Since the spicules are concentrated on the borders of the super-granulation cells, and since these are oriented at random, a stochastic propagation process in established with a diffusion coefficient which depends on the drift velocity. The process may be very efficient for very thin layers, but when a layer is wider than the gyroradii of particles, the drift is very slow. Above this region, in the corona, particles cannot be transported in this form and become stored in the coronal field, where they escape into interplanetary space. Using Reid's (1964) solution for isotropic diffusion and the derived diffusion coefficient, they are able to reproduce azimuthal gradients, and therefore, explain properties (a) to (c), as well as property (h) in relation to the decrease of the spectral index as longitudinal separation from the flare increases. However, unless the width of all the sheets is smaller than the gyroradii of all particles, this process is very inefficient for low-energy particles, which introduces a strong energy-dependence on the propagation process, in addition to the velocity-dependence on the diffusive nature of the process, if the drift were similarly efficient for all particles.

(5) Gold *et al.* (1977) gave a qualitative proposal to explain the shift in longitude of the peak intensity of the 10 April, 1969 event. They suggest that the hot plasma which is ejected by the flare blows the field lines open over the flare site allowing for the escape of energetic particles, and even emission of an enhanced solar wind. Since the flare is within an active center, the magnetic field is quite strong. After a short time the field closes, avoiding easy escape for those particles which are being produced in the flare after the closure. Therefore, particles need to propagate in longitude while they are gradually liberated. On their way, they find localized regions of weak fields or open field lines where they escape easily, giving rise to the shift of the peak intensity. At a distance of about 100° there is one such region beyond which particle transport becomes strongly restricted, to the extent that particles end up escaping from that site. This model explains properties (b) and (g).

Since in a static magnetic field, the higher the particle energy the faster the propagation is, the only option that does not introduce dependence on particle energy is the drift by an electric field. However, if there were an azimuthal electric field throughout the solar plasma, thermal particles would move in absence of flares, unless those electric fields would appear around the site of flare occurrence and disappear some time after the flare. On the other hand, for a diffusion process to be independent of particle velocity, the mean free path λ must behave as $\lambda \propto v^{-1}$. Therefore, although the above possibilities cannot be completely rejected, it seems scarcely probable that static magnetic fields may

explain property (e). The most promising possibility for that goal is to evoke the dynamical behavior of solar magnetic fields; i.e., that the magnetic fields themselves move, carrying with them particles of all energies, at the same rate. The following models were developed in that direction:

(6) The Newkirk and Wentzel Bird-Cage Model: Analogous with bird cages, these authors base their model on the image of a row of cages with adjoining closed doors. In the central cage all kinds of birds are enclosed; suddenly the two doors on both sides are opened allowing the birds to move into lateral cages that have contiguous open doors. However, the doors on the opposite sides remain closed. When the slower birds have entered into those cages, the open doors close and the doors of the other extreme open, so that the birds move into the adjoining cages, and so on. A single case is never connected by both sides, but only one at a time. In this way, all the birds will travel the length of the row of cages at the same effective velocity. Now, imagine instead of birds and cages energetic particles and magnetic archs. Since the arch roots are in stochastic motion due to photospheric motion, Newkirk and Wentzel (1978) proposed that when the roots of two magnetic archs come into contact, there is a topological instability that leads to field line reconnection, allowing the interchange of particles between the two archs over a short time, before they separate again. Such transport is restricted because the particle transmission time must be shorter than the reconnection time, and the second must be shorter than the diffusion time for the stochastic process which may bring them into contact, so that no more than two archs may be simultaneously connected. In this way, the transport process is highly efficient, with a propagation velocity which is energy-independent. During this transport process, particles may escape by gradient and curvature drifts that depend on particle energy, but this energy-dependent escape is limited by a threshold in energy, imposed by the diameters of the archs, limiting the particles to drift within their remain time in a single arch. This model is able to explain property (e) for both low- and high-energy particles if the diameter of the archs is on the order of 10^{10} cm. However, it seems difficult to accomodate the required conditions fortuitously to satisfy every solar particle event. A high number of magnetic flux tubes may be simultaneously present over a large longitudinal extension, with continuous reconnections taking place in only two arch at a time.

(7) The Schatten and Mullan Magnetic Bottle Model: based on the fact that magnetic bottles expanding with velocities of several hundreds of km s^{-1} seem to be a general phenomenon associated with solar flares (e.g., Sakurai, 1965, 1973; Schatten, 1970), azimuthal expansion may be inferred from the Moreton wave associated to type II bursts. Schatten and Mullan (1977) proposed a two-step coronal transport model where the dynamic behavior of the magnetic field during the first step produces similar azimuthal transport for all energy particles. Therefore, when a flare takes place in a closed magnetic field configuration of active centers, the field lines are pushed out of that region, because the kinetic energy of the superheated ejected plasma is higher than the magnetic energy. The flare-accelerated particles remain trapped at the top of the expanding bottle, while bouncing in the photospheric roots of the field lines. The external plasma of the expanding bottle is compressed as the bottle expands more and more,

whereas the internal plasma becomes less and less dense. Due to the force of gravity a Raleigh–Taylor type instability occurs, which produces an exchange between the external and internal plasma. The external field lines become deformed allowing particle escape, while the internal field lines undergo reconnection by topological instability, with the subsequent escape of particles. Particles of energy $E > 3$ GeV may drift out of the bottle before it is opened. The onset time for the trigger of Raleigh–Taylor instability is on the order of 10–1000 s. For the bottle to be completely open it takes an additional 100–2000 s, so that all particles are convected with the same expansion velocities for an interval of $\sim$ 5–50 min. (average of 10^3 s) before their release. According to this model, there are two populations of energetic particles: the first is trapped inside the bottle for a finite time, while continuously accelerating to balance adiabatic losses. This component is liberated once the bottle is opened; the second population is accelerated in the reconnection process when the bottle opens. Relativistic electrons associated with type IV emission are accelerated in this last process. The occurrence of a particle event depends on whether the conditions are given or not for the opening of the bottle, which in turn depends on whether the duration of the flare-induced coronal shock is longer than the Raleigh–Taylor instability growth time. Therefore, when the bottle opens and particles leave this kind of FPR from the top of the bottle, some of them escape directly into interplanetary space and others undergo the second step of coronal transport outside of the FPR. For this last step, Mullan and Schatten (1979) proposed that particles travel through a large-scale coronal field with a superposition of scatter centers. These identify with the network of brillant points seen in X-rays throughout the solar disk, and presumably represent localized enhancements of magnetic field. They carried out numerical calculations of particle trajectories in this static magnetic field, and found that transport is performed by azimuthal drift guided by the general solar magnetic field, while diffusion occurs throughout the assumed network of scatter centers, as proposed previously by Reinhard and Wibberenz (1973); but whereas in the previous model transport is velocity-independent and energy-independent, here both the drift rate and the diffusion coefficient are energy-independent but velocity-dependent. Diffusion dominates low energies and drift dominates high energies. So, the propagation time of low-energy particles from the time of acceleration until particle escape is composed of two parts: $t \simeq t_0 + A/\beta$.

The first term represents the time that particles remain in the bottle, and the second the diffusion time, so that this composition gives a velocity dependence weaker than v^{-1}, as was found by Ma Sung (1977). This model is able to explain properties (a), (b), (c), (d), and (e) in a qualitative manner, and predicts a change in the direction of drift motions every new solar cycle. The predicted time-scales of this model has been critizised by Cliver *et al.* (1982) and further consistently answered by Mullan (1983).

Finally, it must be pointed out that given the degree of uncertainty with respect to some of the listed coronal transport properties and given that we are not yet able to unambiguously separate propagation effects from escape effects, it is not yet possible to adequately judge a given model to prove or disapprove it in a definitive manner. Nevertheless, with the aim of profoundly studying coronal transport, we have developed

a model based on several emission phases, which we have tried to describe as quantitatively as possible.

5. The Multi-Emission Phase Model of Particle Coronal Transport

Taking properties (d) and (e) as starting points, we can assume that the coronal magnetic field must play an active role in the transport of solar flare particles; i.e., the fields must have a dynamic character. Otherwise, if the static magnetic fields were prevalent anywhere, coronal injection profiles would present a characteristic velocity dispersion and energy and rigidity dependence that is not observed in the main particle population (≤ 100 MeV). With dynamic fields it is possible to search for situations where all kinds of particles are constrained to similar transports but since according to property (e) there is a slight dependence on velocity in the transport process, it is probable that dynamic fields are not present through all the traversed regions from the point of particle acceleration to particle injection in interplanetary space. One possibility is that propagation may be of a different nature in different coronal regions. We know from property (d) that particle transport within the FPR is carried out at a rate different than transport outside the region. Since many of the observable events are associated with flares whose connections with the observant are located within the range of longitudes of the FPR, and given that energy and rigidity independence is observed in most particle events, it is usually assumed that velocity-independent transport is a property of the FPR, whereas the slight velocity dependence of low-energy particles is acquired outside of that region. Furthermore, since properties (a), (b), and (c) appear to be the result of a diffusive-like-process, and according to property (g) peak intensity may shift in heliographic longitude from the flare site, it seems natural to infer that any velocity-dependent process occurs outside of the FPR. Therefore, following Schatten and Mullan (1977) we assume that transport in the FPR is performed in association with a dynamic magnetic field where particles are contrained. Furthermore, according to Reinhard and Wibberenz (1974) we assume that transport outside the FPR is dominated by drifts and diffusion. We attempt here to give a global model for explaining the general features of coronal transport, rather than particular behavior of solar particles in a specific solar flare event.

5.1. Qualitative description of the involved physical processes

The temporal and spatial sequences of different emissions during a solar flare have led to a widely accepted description of the flare phenomenon in four main steps: the pre-flare phase, the impulsive phase, the flash phase, and the main phase (e.g., Priest, 1981). Microwave impulsive bursts and hard X-rays are evidence of energetic electron production during the impulsive phase. On the other hand, there are inferences that high energy protons even (multi-GeV protons) are already present in flare regions at the beginning of the flash phase (Chupp and Forrest, 1982), and that the injection of protons of 4–80 MeV may be instantaneous within the time-scale of the flash phase (e.g., Ma Sung *et al.*, 1975). Therefore, it seems that the first acceleration stage takes place during the impulsive phase and is probably caused by a deterministic acceleration process.

According to Pérez-Peraza *et al.* (1977, 1978) if the impulsive process is associated with neutral current sheet acceleration, multi-GeV protons can be obtained in some seconds. Therefore, we assume that the flare process is generally initiated in a closed magnetic field configuration. Flare energy is so large, that within the time-scale of the impulsive phase, energy density of the plasma and accelerated particles may be higher than magnetic energy density ($\beta \geq 1$). According to statistical studies of Hudson (1978) and Belovskii and Ochelkov (1980), $\beta \geq 1$ in a high number of solar flares. Under these circumstances, $\beta > 0.1$–0.3 is sufficient for the magnetic trap to be destroyed by the effect of an MHD-instability, or because of an absence of equilibrium (e.g., Parker and Stewart, 1967; Meerson and Sasarov, 1981). Following trap destruction an appreciable amount of plasma with energetic particles and frozen-in magnetic fields is ejected from the magnetic trap on a time-scale, $\tau_{tr} = L/V_A$, where L is the characteristic size of the trap and V_A the Alfvén velocity. Therefore, if the flare region is located, for instance, at a height of 0.005–$0.05\ R_\odot$ above the solar surface, and has an average longitudinal size $\sim 10°$, then $L \sim 10^{10}$ cm in such a way, that assuming hydromagnetic motions of ~ 1000–2000 km s^{-1}, we obtain $\tau_{tr} \simeq 50$–100 s, which is on the order of the time-scale of the impulsive phase. Afterwards, the field lines may close again, since magnetic field strength is usually very high in those active centers. Particle release in this phase, while depending on energy density of the accelerated particles, is independent of particle energy. Later, in the course of the flash and main phases of the flare, more hot plasma of very high conductivity is created, so that frozen plasma and field expand outwards as the kinetic pressure in the interior of the closed loops increases. With this, the condition is such that $\beta < 0.1$–0.3, in which case according to Meerson and Sasarov (1981) magnetically trapped particles excite strong Alfvén wave turbulence of a small transverse scale. According to Pérez-Peraza (1975) small scale turbulence of linear dimensions ~ 1–10 km may account for effective stochastic acceleration up to some GeV in a time-scale of about ~ 20 s, if this second acceleration stage has taken place on chromospheric levels. If the second step has taken place on a coronal level, according to Mullan (1976, 1983) a high-pressure piston is formed which drives a shock within the closed field configuration. Magnetized turbulent cells of a scale size of ~ 100 km remain bound in the wake of the 'bottled up' shock wave. Since shock-wave velocity is greater than the expansion velocity of the magnetic bottle, statistical Fermi acceleration overcomes the first order of the Fermi process (adiabatic losses) due to the expansion of the bottle; this second acceleration stage, initiated in the flash phase, is prolonged until the shock wave disappears, or the confinement of particles in the bottle is no longer effective. Though there is a time interval between the onset of the first acceleration stage and the onset of the second acceleration stage, in some events these may occur in a superimposed fashion; i.e., the second stage may have initiated before the first stage is completed. If the flare magnetic configuration is broken in the impulsive phase, some of the energetic particles are impulsively ejected into interplanetary space and others remain in the environment of the active region. In this way, at the beginning of the particle event there is a strong anisotropy aligned with interplanetary field lines. This is connected to the heliographic longitudes of the cone which is displayed by the

open lines, i.e., azimuthal distribution is determined by the extension of the fan-type cone of open lines. The accelerated electrons reach lower energies than protons because they are strongly decelerated in the source medium. In fact, while protons only lose energy by collisional and adiabatic losses and energy degradation by p–p collisions, electrons lose energy by collisional and adiabatic losses, gyrosincrotron, bremstrahlung, and Compton inverse effect. However, for a given energy, electrons arrive at the detection point faster than protons because of a higher velocity. It is predicted that when the first emission phase occurs, maximum peak intensity will be seen at the flare site, even if peak intensity shifts during a later emission phase. The energy spectrum of electrons will show a definite change of slope at a certain energy (~ 100 keV) in some events, indicating two different populations. Those of the primary process accelerated in a dense medium, and those of secondary acceleration in a less restricting medium. For protons, the change of slope may take place at some MeV, however, the break in the spectrum is not very abrupt because low-energy protons from the first emission mix with the first released protons of the second emission in the connecting longitudes with the flare site, arriving at the observation point at the same time.

When flare conditions are such that the magnetic trap is not destroyed in the impulsive phase ($\beta < 0.1$–0.3), the population of the first acceleration process mixes with the population of the secondary acceleration in the loop, remaining confined in the expanding bottle. In this case, no noticeable change in slope is predicted in particle spectra, and the maximum peak intensity will not necessarily occur at the flare site. In such a case, an early flux of low-energy electrons is not expected. Obviously, when the conditions for the opening of the expanding bottle are not replenished as discussed by Mullan (1983), only the impulsive component emitted during the impulsive phase will be observed as an event with a small emission cone. In addition, if the conditions of the break down of primary source configurations during the impulsive phase did not occur, no particle event is expected.

5.1.1. *Velocity Independent Transport of Low-Energy Particles in the FPR*

Among the particles that are impulsively ejected in the first emission phase, as mentioned before, some reach the interplanetary field lines and energy-independently. So, only interplanetary propagation is important, while the others remain trapped in the local fields where they may be re-accelerated to high energies in a second acceleration stage, during the course of the flash and main flare phases. Stored particles and the newly accelerated components in the expanding bottle might be scattered by Alfvén wave turbulence and precipitate into the dense atmospheric layers as a consequence of cyclotron instability (Kennel and Petschek, 1966). This instability arises due to anisotropy of longitudinal and transversal pressures of high-energy particles with respect to the magnetic field in the bottle. However, according to Meerson and Rogachevskii (1983), particle precipitation does not occur if the characteristic life time of particles in the trap is longer than wave-passage time ($\tau_{\varpi} = h/V_A$), where h is the height of the arch, i.e., that the characteristic time of particle diffusion is longer than τ_{ϖ}, in which case particles remain stored for long time, and do not precipitate into dense

regions. The conditions for storage is reduced to $\beta < \beta_*$, where β_* is a value that increases along with the distance from the photosphere. Since β decreases with height above the photosphere as internal density decreases with the expansion of the bottle, this suggests that as the bottle expands, particles have a lesser probability of becoming lost in the dense layers of the solar atmosphere.

Longitudinal and radial expansion of the magnetic bottle, as well as the subsequent opening by a Raleigh–Taylor instability, followed by field line reconnection have been widely described by Schatten and Mullan (1977), and Mullan (1983). Such an expansion produces convective particle transport in a manner independent of energy and rigidity. However, particles of $E \geq 100$ MeV may occasionally escape from the trap by drifts from magnetic field gradient and curvature which are velocity-dependent, $V_d = (\gamma_L mc/q^* R_c H)\ (v_\parallel^2 + v_\perp^2/2)$, where m, p^* and γ_L, are the particle mass, effective charge and Lorentz factor, respectively; R_c, the radius of the bottle; H, the field strength; $v_\parallel$ and $v_\perp$, the parallel and perpendicular components of particle velocity in relation to the magnetic field. Combining $v_\parallel$ and $v_\perp$ into an effective total velocity v, we have for 100 MeV protons $v = 1.285 \times 10^{10}$ cm s^{-1}. According to Mullan (1983), the radius of the bottle at the time of its opening is 0.05–0.5 $R_\odot$, so it can be shown that high-energy particles may drift prior to the opening. For instance, if we take $R_c = 0.01\ R_\odot$ when the bottle opens at 0.05 $R_\odot$ and $R_c = 0.1\ R_\odot$ when it opens at 0.5 $R_\odot$ we have 100 MeV protons escape after $t = 0.5$–5 min. if $H = 1$–10 G, respectively, in the first case, and $H = 0.1$–1 G in the second case. When the bottle is about to be opened $R_c \sim 0.05$–0.5 $R_\odot$, (1 and 0.1 G, respectively), enclosed particles begin to escape by drifts after a time of about 13 min (if the bottle has not yet opened). Therefore, in those cases, it is expected in some particle events that particle escape of high energy protons be definitively energy-dependent. Meanwhile, the net transport of the bulk of particles is that of the expanding region with a relatively high velocity. At the end of the convective motion, particles have completely filled the top of that FPR, so that when the bottle opens, the next transport step initiates at the coronal level of the bottle opening for those particles that do not escape directly.

5.1.2. *Velocity-dependent transport out of the FPR*

Once particles leave the bottle, transport is accomplished by drifts and diffusion, while particles escape as they find preferential sites of open field lines, according to the field topology behavior in each particular event. The basic motion of particles runs along the north–south general magnetic field of the Sun. So, the gradient and curvature drifts of particles travelling along that field are in the azimuthal direction, depending on the charge, ad mass and velocity of the particles. For the diffusion process, alternatively with the possible static scatter centers associated with X-rays bright points, the flare disturbance may affect the solar corona at heights so extended as 1 $R_\odot$. So, coronal magnetic fields are disturbed at least for some time after the flare. Such irregularities may act as diffusion centers, making possible azimuthal transport in addition to drifts. However, at heights far above 1 $R_\odot$, the fields must be more ordered and transversal diffusion may be negligible in relation to radial motion, Therefore, the propagation

region is composed of a background of ordered magnetic fields, superimposed by magnetic irregularities of all scale sizes. According to Parker (1963), particle transport in disorder fields is described by means of two transport geometries, the thick or thin geometries if particle gyroradii are smaller or larger, respectively, than the average size of field irregularities, and a drift geometry in ordered magnetic fields. The diffusion coefficients in thick and thin geometries and the drift rate may be generalized in the following expression:

$$\kappa_L \sim (q^*/A)\mathbf{R}^L \sim (Z/q^*)\beta^L,$$

where $L = 1$, 2, and 3 correspond to the thick, drift and thin geometries respectively. $\mathbf{R}$ is magnetic rigidity, A and Z are the atomic mass and atomic number, $q^* \sim Z[1 - \exp(-130\beta/Z^{0\sim 66})]$ is particle effective charge and β is particle velocity in terms of light velocity. Assuming that the average magnetic field strength of the field concentrations at $\sim 1\, R_\odot$ is of 10 G (or ~ 1 G), and their diameter of ~ 1 km (or ~ 10 km), protons with energies lower than ~ 100 MeV move in a thick geometry ($\kappa_1 \sim \beta$), whereas protons of $E \gtrsim 100$ MeV move in a thin geometry ($\kappa_3 \sim \beta^3$). According to observational properties (a), (b), and (c), the azimuthal transport shows a typical behavior of diffusive propagation. However, if azimuthal transport were exclusively accomplished by diffusion, the travelling time would present velocity dependence in the form $t \sim 1/v$. On the other hand, according to property (g) a collective motion of particle fluxes seems to be superimposed with diffusion, producing a shift in the peak flux. Assuming that a drift of particle fluxes may be inferred from that coherent shift as proposed by Reinhard and Wibberenz (1973), the transport time in the LPR (since particles leave the magnetic bottle until they escape) can be expressed as the sum of the two following components, under the consideration $t \sim 1/\kappa$:

– low-energy protons:

$$t_{\mathrm{LPR}} = t_{\mathrm{thick}} + t_{\mathrm{dr.}} \sim \beta^{-1} + \beta^{-2} \sim \beta^{-1},$$

– high-energy protons:

$$t_{\mathrm{LPR}} = t_{\mathrm{thin}} + t_{\mathrm{dr.}} \sim \beta^{-3} + \beta^{-2} \sim \beta^{-2},$$

which is similar to the conclusion of Mullan and Schatten (1979) – diffusion with a velocity-independent mean free path is dominant at low energies; whereas drifts are the dominant transport processes at high energies – that is, high-energy protons are transported to longer distances from the flare site than low-energy protons. The superimposition of diffusion and drift of low-energy protons gives, as we have seen, a velocity-dependence in the form of $t \sim v^{-1}$. However, according to property (e) their velocity-dependence during coronal transport is of the form $t \sim v^{-0.55}$. Nevertheless, this may be conciliated from our preliminary assumption that transport in the first emission phase and in the FPR is velocity-independent, to the extent that the resultant velocity-dependence from the combination of both propagation regions is:

$$t_{\Psi} = t_{\mathrm{FPR}} + t_{\mathrm{LPR}} \sim \text{const.} + v^{-1} \sim v^{-\mathbf{q}} \quad \text{with } (0 < \mathbf{q} < 1),$$

which is just what is claimed in property (e) for low-energy protons. For high-energy protons we have:

$$t_{\Psi} = t_{\mathrm{FPR}} + t_{\mathrm{LPR}} \sim \text{const.} + v^{-2} \sim v^{-\mathbf{h}} \quad \text{with } (1 < \mathbf{h} < 2).$$

Therefore, azimuthal transport of high-energy protons is quasi-energy and rigidity dependent, since for a given field geometry the drift velocity behaves as

$$v_d \sim (c/q^*)mv^{\mathbf{p}} \quad (\mathbf{p} > 2).$$

It is worth mentioning here the general features of spectral shape behavior as described in property (h): In some events, during the first emission phase of the narrow emission cone, particles of all energies are concentrated in that cone around the flare site in such a way that there are relatively more high-energy particles within the corresponding narrow cone of detection than afterwards, when the magnetic bottle opens and high-energy particles are found distributed over a much wider emission cone of at least the longitudinal extension of the opened bottle. For this reason, there are relatively less high-energy particles far from the flare site in the initial phase of particle events. In addition, protons of $E > 100$ MeV have occasionally escaped in an energy-dependent manner before the bottle opens. Furthermore, a high concentration of low-energy particles may be expected during the second acceleration stage in the bottle due to adiabatic losses. These are the predicted reasons why the energy spectrum becomes steeper with longitudinal distances from the flare site. However, in events where there is no first emission phase, a noticeable increase of the spectral index with azimuthal distance is not expected in the initial phase of the particle event, at least for energies lower than 100 MeV. In the decay phase of the event, the decrease of the spectral index in distance from the flare is due to the drift effect which preferentially carries high-energy protons away long distances, so that after a long time there are relatively more high-energy particles farther from the flare than around the FPR where they were liberated.

Propagation out of the FPR is not completely uniform throughout the solar disk, but the fluxes are modified when particles pass from one sector of a given magnetic polarity to a sector of opposite polarity. In fact, according to the description of Svalgard *et al.* (1974) of the coronal magnetic field structure over sector boundaries, there is a neutral current sheet lying along the sector boundary. Therefore, the diffusion coefficient and drift rate are modified when particle fluxes reach a sector due to a drift-like process along the neutral sheet, similar to the process suggested by Fisk and Schatten (1972).

5.2. Quantitative predictions of the model

Assuming that propagation of the impulsively ejected particles in the first emission phase, during the impulsive phase of the flare, is purely interplanetary propagation, we will concentrate on the second emission phase, when particles undergo azimuthal coronal transport. We have already mentioned that velocity-independent transport in the FPR is associated with a convective process produced by flare phenomena, such as an expanding magnetic loop, or alternatively, the expulsion of a hydromagnetic shock

(the flare blast wave) keeping particles under acceleration behind the front shock, until they reach a height of 0.5–1 $R_\odot$, where there is no longer a very high concentration of closed magnetic field archs, and where the changes in thermodynamic parameters, and thus in conductivity, may lead to the defreezing of field lines, and liberation of the constrained energetic particles. Meanwhile, net transport of all particles is in the expanding region, so, we assume a convective-like process where particles propagate coherently at a definite velocity v_c. The evolution of the number density of particles at a point X and a time t within the FPR is expressed in unidimensional coordinates, by the condition of particle conservation (Pérez-Peraza and Martinell, 1981):

$$\frac{\partial N}{\partial t} = -v_c \frac{\partial N}{\partial X}. \tag{1}$$

For the task of mathematical simplicity, we have neglected collisional and adiabatic losses, as well as the second acceleration process rate, under the rough assumption that there is an equilibrium between energy gains and losses. We also assume that Equation (1) is concerned mainly with the bulk of flare particles (≤ 100 Mev), since an additional term for the energy-dependent escape rate should be included for higher energies. A similar analysis in spherical coordinates has been previously developed by Martinell and Pérez-Peraza (1981). The solution of equation (1) gives a coherent pulse of particles in the azimuthal direction X in the form:

$$N(X, t) = \frac{N_a}{X_0} \delta(X - X_f - v_c t), \tag{2}$$

where N_a is the number of accelerated particles, X_0 the FPR extension and X_f the flare extension assumed to be symmetric with respect to a localized origin. Since coherent motion takes place in all directions, the convected energetic particle fluxes distribut uniformly at the top of the FPR, so that the initial conditions for transport outside are:

$$N(X, 0) = \begin{cases} N_a/X_0\,, & -X_0/2 \leq X \leq X_0/2\,, \\ 0\,, & |X| > \pm X_0/2\,. \end{cases} \tag{3}$$

Once particles abandon the FPR volume, they are conveyed by diffusion with a diffusion coefficient k_l, and by drift at a velocity V_d, and are lost in the interplanetary space at a rate Γ (e.g., Reinhard and Roelof, 1973). The corresponding transport equation, neglecting energy losses, corrotation, and flux depletions for changes through different unipolar magnetic sectors, is:

$$\frac{\partial N}{\partial t} = k_l \frac{\partial^2 N}{\partial X^2} - v_d \frac{\partial N}{\partial X} - \Gamma N. \tag{4}$$

It must be pointed out that Equation (4) also applies to heliographic longitudes located above the FPR. The difference between Equation (1) and Equation (4) is that they operate at different heights in the corona and at different times. The analytic

solution of Equation (4) is:

$$N(X,t) = 2.5N_a \exp\left(-\Gamma t - \frac{(X - v_d t)^2 + (X_0/2)^2}{8\kappa_l t}\right) \times$$

$$\times \left\{ \exp\left[\frac{(X - v_d t)(X_0/2)}{4\kappa_l t} + \frac{(X - v_d t - X_0/2)^2}{8\kappa_l t}\right] \mathrm{erf}\left(\frac{(X - v_d t - X_0/2)}{(4\kappa_l t)^{0.5}}\right) - \right.$$

$$\left. - \exp\left[-\frac{(X - v_d t)(X_0/2)}{4\kappa_l t} + \frac{(X - v_d t + X_0/2)^2}{8\kappa_l t}\right] \mathrm{erf}\left(\frac{(X - v_d t + X_0/2)}{(4\kappa_l t)^{0.5}}\right) \right\}. \quad (5)$$

It can be appreciated from Equations (3) and (4) that solution (5) does not depend on the convective velocity v_c and the source location X_f, and that κ_l and v_d are implicit functions of particle kinetic energy E. Assuming that the FPR liberates the flare particles at a height of 0.8 $R_\odot$ above the solar surface, we have translated the linear coordinates into angular coordinates by the relationship $\Psi = (X/1.8\,R_\odot)57.295$. In accordance with previous studies of coronal transport, let us assume a coronal drift velocity $v_d = 4 \times 10^6$ cm s^{-1}, $\kappa_l = 2 \times 10^{17}$ cm^2 s^{-1} for protons of $E > 50$ MeV and $v_d = 4 \times 10^5$ cm s^{-1}, and according to Ng and Glesson (1976) $\kappa_l = 2 \times 10^{16}$ cm^2 s^{-1} for protons of $E \leqslant 50$ MeV. For the loss rate we used $\Gamma = 3600$ s^{-1}, but the model is weakly sensitive to variations of Γ within a factor of 100. The results shown in the next figures are given in terms of $N(X,t)/N_a$. Figure 2 shows the azimuthal distribution of

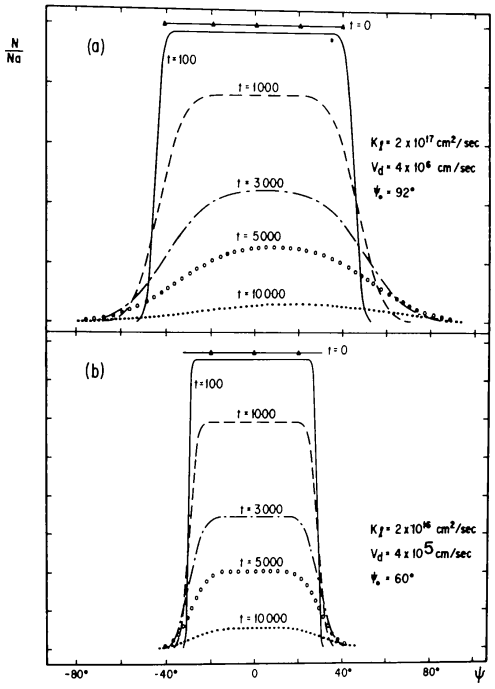

Fig. 2. Azimuthal distributions of high-energy (a) and low-energy protons (b) from the opening of the FPR up to 10^4 s. The drift effect predominates at high energies and late times.

particles in the corona given by Equation (5). On the upper panel we considered high-energy protons and a FPR extension $\Psi_0 = 92°$, while the lower panel corresponds to low-energy protons and $\Psi_0 = 60°$. It can be noted that according to property (c), the angular distribution tends to be uniform for a very long time, as well as a certain shift of the peak intensity of the flare site (normalized at $\Psi_f = 0°$) as indicated by property (g). This east–west drift is seen in panel (a), for high-energy protons for a relatively long time, however, the shift is less noticeable at low energies, indicating the relative importance between drift and diffusion changes with velocity. In figure 3 the coronal

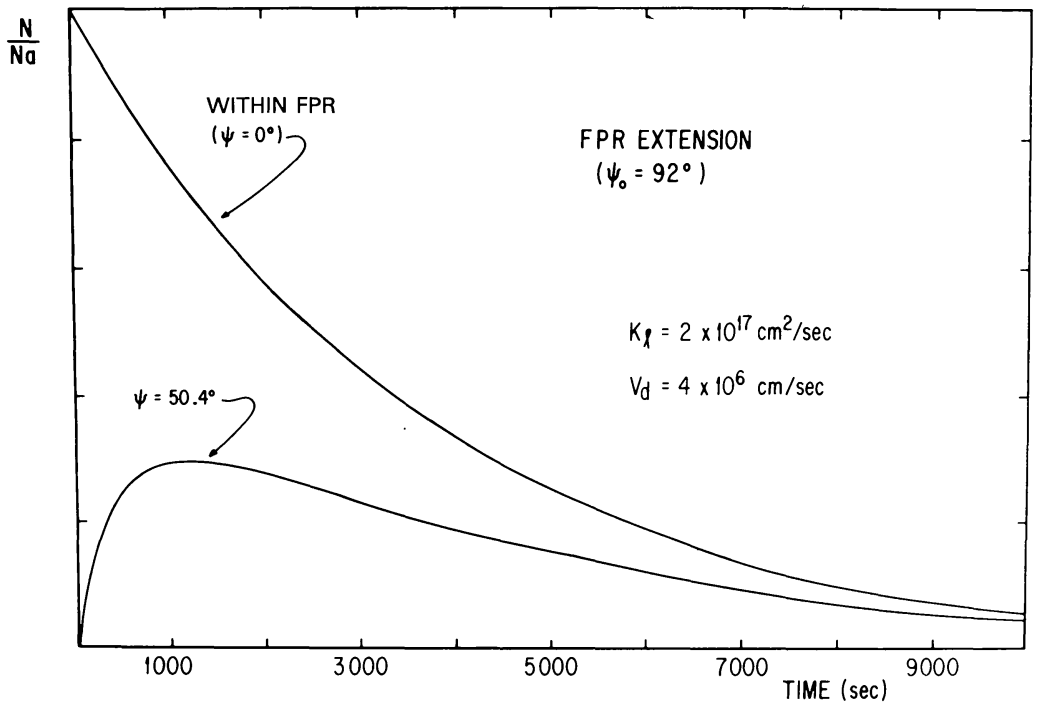

Fig. 3. Coronal time profiles of high-energy protons at two different longitudes: above and at the center of the FPR, and out of the FPR (50°.4) where the profile takes a diffusive-like form.

injection time profiles of high-energy protons is shown for two different heliographic longitudes: one above the FPR, and the other just outside of the FPR extension, for $\Psi_0 = 92°$. It can be appreciated that in the LPR, at a longitude $\Psi = 50°.4$, the intensity-time profile is typical of the diffusive-type, whereas above the FPR, just at the center of the flare site, $\Psi = 0°$, the profile is quite different. It may also be noted that according to property (a), the peak intensity is shifted over a later time with azimuthal distance; according to property (b) the profile widens with separation from the flare site, and according to property (c) the intensity tends to be equal at both locations for a late time. Figure 4 shows similar behavior of the coronal injection profiles of high-energy protons for a FPR extension $\Psi_0 = 100°$, and two different locations, one within the FPR at $\Psi = 40°$, and the other outside the FPR at $\Psi = 55°$. Therefore, these results represent particle distributions reaching the roots of the interplanetary field lines, but not the observed fluxes. To reproduce the observational fluxes at the Earth's orbit, we must incorporate interplanetary effects. Since interplanetary transport is radial along the field

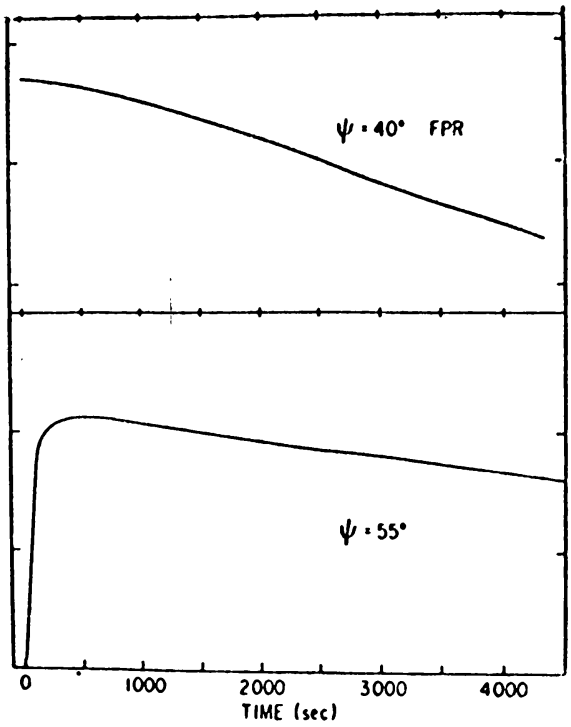

Fig. 4. Idem Figure 3 with a FPR extension of 100°: $\Psi = 40°$ is within the FPR and $\Psi = 55°$ is out of the FPR.

lines, the longitudinal distributions at the coronal escape remain basically unaltered. So, with the aim of illustrating a translation of the injection profiles to the level of the Earth's orbit, we have chosen the simplest diffusion description along magnetic flux tubes, with a constant magnetic diffusion coefficient K. According to Parker (1963), particles that are impulsively ejected from the Sun are distributed in interplanetary space, at the level of the Earth's orbit in the following form:

$$U(r, \tau) = \frac{N_a}{(4\pi K\tau)^{\eta/2}} \exp(-r^2/4K\tau), \tag{6}$$

where τ is the interplanetary travel time, η is the degree of freedom ($\eta = 3$), N_a is the number of impulsively ejected particles and $r = 1.2$ AU is the distance from the upper corona along an interplanetary field line. When ejection is not impulsive but gradual during azimuthal transport, the observed time profile is obtained from the convolution of Equation (6) with the injection profile given by Equation (5). So, the observed particle profile is:

$$W(\Psi, r, t, \tau, E) = v\frac{N(\psi, t-\tau, E)}{(4\pi K\tau)^{\eta/2}} \exp(-r^2/4K\tau) \text{ (protons MeV}^{-1}\text{ s}^{-1}\text{ cm}^{-2}\text{ster}^{-1}), \tag{7}$$

where v is the velocity of particles and $(t - \tau)$ is the particle coronal travel time. Taking $K = 5 \times 10^{21}$ cm^2 s^{-1}, we show in Figure 5 the results of this convolution for the two

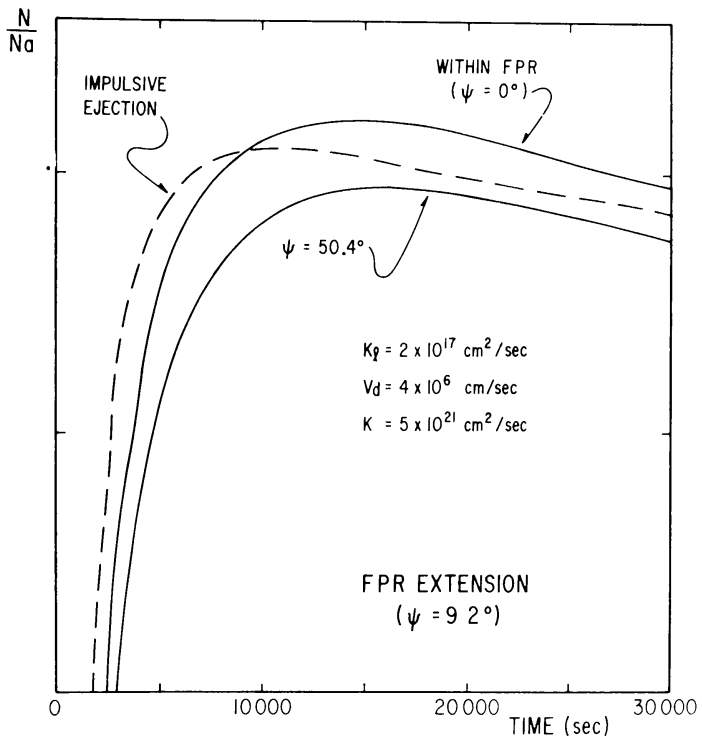

Fig. 5. Time profiles at the Earth's level according to the convulution of the coronal injection profiles of Figure 3, relative to impulsive ejection from the flare site, as if it were not a FPR.

profiles of Figure 3. We have plotted the profile of pure interplanetary propagation for comparison as if particles were impulsively ejected. It can be appreciated that though the shapes of the coronal profiles are lost (this is more noticeable for longitudes located within the FPR at $\Psi = 0°$, for instance), the shifts at the onset and the peak intensity times and the broadening of the profile with azimuthal separation – i.e., properties (a), (b), and (c) – are conserved through interplanetary propagation, and are displaced relative to impulsive ejection. Similar results are obtained with low-energy protons, but with a delay in time-scales. In the case of particles from the first emission phase (during the flare impulsive phase), dashed curves represent typical time-intensity profiles.

5.2.1. *Application and Implications of the Model to Specific Proton Events*

Now that we have shown that the proposed model is able to describe most of the general features of azimuthal particle transport which are common to most solar events, we will apply it to some specific events to test if those features are adequately described within the time-scale of events, and afterwards we will draw some inferences on the source characteristics of particle fluxes. Since we do not dispose of particle flux data at the coronal level to test our predictions for each event, nor enough data on coronal dynamics during those events to derive reliable particle fluxes at the level of the roots of interplanetary field lines which could be modulated for interplanetary transport and be compared to observational fluxes, we will proceed in the opposite fashion (Pérez-Peraza *et al.*, 1985). We consider the demodulated data for interplanetary propagation of several proton events as given by Miroshnichenko (1985) and Miroshnichenko and

Petrov (1985). These data furnish the energy spectra at the moment of particle ejection from the solar corona in a limited range of particle energy, according to limitations of observational data. We demodulate those coronal fluxes for coronal transport to return back to the source, and in this form we derive a source energy spectra that can be compared with those obtained from solar neutrons and γ-ray lines. Yet, most of our results are not testable but rather of a predictive nature, because we dispose of source data only for a few events.

We assume that demodulated observational particle flux proceeds from a coronal longitude of $X_c = 60°$ W, and has been ejected from the corona at time (t_e), given as $t_e = 0$ if $|X_c| \leq X_0/2$ and $t_e = |X_c|/v_d$ if $|X_c| > X_0/2$. Next we equate Equation (5) with the energy spectrum $N(E)$ demodulated for interplanetary transport:

$$2.5N_a(E)\,\{f[X_c, t_e, v_d(E), \kappa_l(E), X_0]\} = N(E)\,(\text{protons MeV}^{-1}), \tag{8}$$

where the function f corresponds to the normalization of Equation (5) relative to its maximum value; i.e., when the flux is maximum at time t_e immediately after $t_e = 0$, over the top of the FPR. The employed spectra $N(E)$ at the level of the roots of interplanetary field lines have been translated from magnetic rigidity to kinetic energy, as is shown in Figure 6 and 7 and Tables I and II. Since we do not dispose of observational informa-

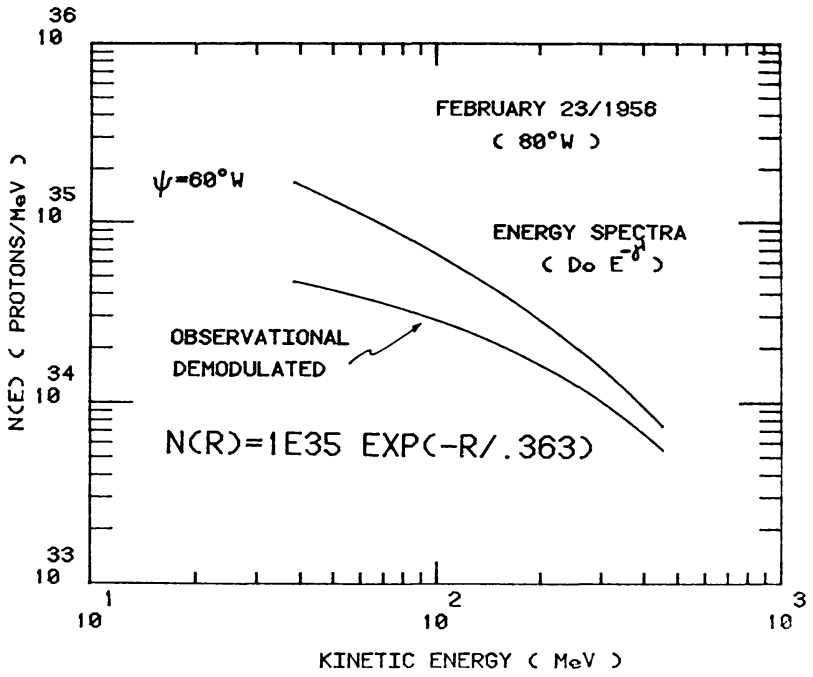

Fig. 6. Rigidity spectrum at the level of the coronal roots of the interplanetary field lines and transformation to a power law kinetic energy spectrum of the 23 February, 1956 event.

tion on the size of the FPR in each solar proton event, for the task of simplicity we take the azimuthal width $X_0 = 80°$ at its opening at 0.9 $R_\odot$ above the photosphere, centered at the flare site X_f. Therefore, our results refer to the flare position, X_f, such that $X_i = X - X_f$, e.g., $X_c = X\,(60°\text{ W}) - X_f$. For a sample of events illustrated in Tables I and II we employed $v_d = (60\text{–}250)\beta^2/(1 - \beta^2)^{0.5}$ (cm s^{-1}) depending on whether the

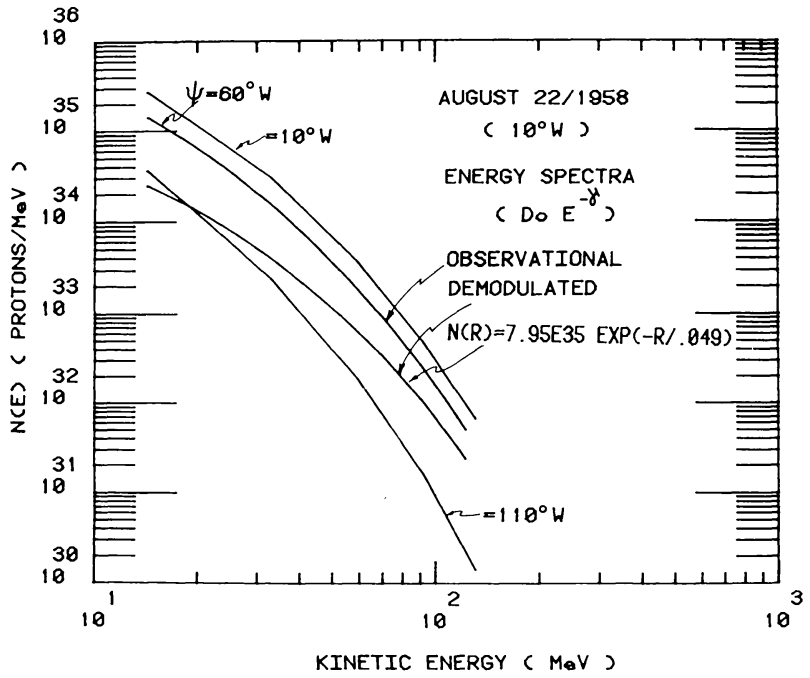

Fig. 7. Rigidity and kinetic energy spectra from interplanetary demodulation at 60° W, of the 22 August, 1958 event, and energy spectra above the FPR at the level of the flare site and 100° to the West.

TABLE I

Source energy spectra from demodulation of data, for events where the FPR ($\psi_f \pm 40°$) contains the Earth–Sun connecting longitude at 60° W

Events	Flare	Ejection time (UT) (60° W)	Source spectrum (protons MeV)		
			D_0	γ	Range (MeV)
23 Feb., 1956	23° N 80° W	03 : 58	1.81×10^{37}	1.24	40 – 500
15 Nov., 1960	23° N 35° W	02 : 37	3.21×10^{38}	2.17	40 – 500
7 July, 1966	35° N 48° W	00 : 56	2.96×10^{36}	3.40	100 – 500
28 May, 1967	28° N 32° W	05 : 59	5.52×10^{33}	2.01	1 –1000
4 Oct., 1968	17° S 36° W	23 : 56	1.86×10^{34}	1.80	10 – 200
18 Nov., 1968	21° N 87° W	10 : 51	6.56×10^{37}	2.51	10 – 60
25 Feb., 1969	13° N 37° W	09 : 29	5.10×10^{34}	1.33	10 – 200
30 Mar., 1969	19° W 90° W	03 : 48	9.97×10^{34}	2.83	90 – 400
2 Nov., 1969	14° W 90° W	09 : 45	5.26×10^{36}	2.90	10 – 60
24 Aug., 1971	18° N 49° W	23 : 47	3.91×10^{39}	2.81	10 – 60
7 Aug., 1972	14° N 37° W	15 : 50	6.17×10^{35}	2.20	0.1– 250

TABLE II

Coronal and source energy spectra of protons from interplanetary and coronal demodulation of data, for events where the Sun–Earth connecting longitude (60° W) is outside of their FPR

Event	Flare site	Hα-time (UT)	Ejection time* (UT) (60° W)		Spectra (protons MeV)				
					Coronal (60° W)		Range (MeV)	Source	
					D_0	γ		D_0	γ
22 Aug., 1958	18° N 10° W		14 : 50	16 : 06	3.70×10^{39}	3.63	15–150	1.72×10^{45}	6.18
3 Sep., 1960	18° N 88° E		01 : 08	02 : 29	1.84×10^{36}	1.93	10–400	2.28×10^{41}	3.93
28 Sep., 1961	13° N 29° E		22 : 23	23 : 09	7.89×10^{38}	3.02	15–550	1.64×10^{43}	4.63
28 Jan., 1967		150° W	07 : 30	08 : 24	5.20×10^{34}	1.25	75–400	3.81×10^{36}	1.82
29 Sep., 1968	13° N 13° W		09 : 40	10 : 39	1.04×10^{34}	1.49	10–200	1.63×10^{40}	4.21
24 Jan., 1969	20° N 08° W		07 : 28	09 : 49	5.24×10^{35}	3.10	10– 60	4.67×10^{43}	7.20
25 Sep., 1969	13° N 15° W		06 : 58	09 : 08	1.28×10^{35}	3.15	10– 60	1.14×10^{43}	7.25
1 Sep., 1971	12° S 130° W		20 : 00	23 : 26	1.43×10^{38}	2.25	10– 60	2.81×10^{46}	6.62
28 May, 1972	09° N 30° E		13 : 32	16 : 44	1.09×10^{37}	2.59	30– 80	4.17×10^{41}	4.61

* This time concerns particles of $E < 100$ MeV, since higher energy particles may have escaped well before, as explained in the text.

observational peak intensity was very late or early respectively, where $\beta = v/c$, v, and c are particle and light velocities.

We used $\kappa_l = 2 \times 10^{17}\beta(\text{cm}^2\ \text{s}^{-1})$ which is just within the range of values derived in an empirical form through different works. From Equation (8) it can be seen that the source energy spectrum is:

$$N_a(E) = N(E)/2.5f(X_c, t_e, v_d, \kappa_l, X_0), \tag{9}$$

which, of course, is independent of the longitude X_i of the coronal flux evaluation, but since the demodulated spectrum $N(E)$ corresponds to 60° W of coronal longitude, we derived $N_a(E)$ from the evaluation at X_c. It should be emphasized that according to this model, if the Sun-Earth connecting longitude X_c is within the FPR extension X_0, the source and the observational spectrum are similar, because of the conditions in Equation (3), so, $N_a(E) \sim N(E)$. However, in general, what Equation (8) means is that the demodulated spectrum at position X_c is produced by the source spectrum and modulated by drifts and diffusion of particles during their azimuthal coronal transport from the top of the FPR to longitude X_c. For simplicity we refer that distance, as we said before, relative to coronal longitude X_f connected to the flare site, so that t_e may be considered as the time of ejection of the maximum flux intensity, at that particular position. Therefore, Equation (9) means that source spectra are obtained by the demodulation from azimuthal coronal transport of the spectra at the root level of the interplanetary field lines, $N(E)$. In Table I we illustrate the case where the Sun–Earth connecting longitude X_c falls within the FPR; in column 3, for the ejection time ($t_e = 0$) we assigned a real value given by a characteristic time of the Hα-flare, as reported in literature, plus 10^3 s, which is the mean time for the opening of the FPR, as discussed before. In columns (5) and (6) we tabulated the parameters of the source energy spectrum $D_0E^{-\gamma}$ which is the same as that at the coronal level for longitudes $X_f \pm 40°$. In Table II, we show our results for a sample of 9 events where the connection point X_c is outside the FPR. Therefore, in the fourth column we tabulated the ejection time at X_c, which is the time elapsed for particles to propagate from X_f to X_c plus 10^3 s, with reference to a characteristic time of Hα-flare as reported in the literature. In column (5) and (6) the parameters of the spectra at the coronal level appear, and in columns (8) and (9) the parameters of the source spectra are listed.

Once we have determined $N_a(E)$ (protons MeV^{-1}) we are able to build the time profiles at the coronal level by fixing the position X_c and energy E_i in Equation (5), and making time vary relative to t_{on}, $(t - t_{on})$, where $t_{on} = (|X_i|/v_d) - X_0/2$ is the onset time of the particle arrival at the particular position X_i, i.e., the arrival time of the first particles at X_i. The particle azimuthal distributions were built by fixing energy and time in Equation (5), and evaluating in $X_i < \pm 180°$, taking the flare position as the origin of longitudinal coordinates, and interating different times and particle energies. We have, translated linear azimuthal positions X_o in terms of angular coordinates Ψ_i to illustrate our results.

In Figure 7 we made use of Equation (8) for the 22 August, 1958 event where the FPR does not contain X_c, to calculate the spectrum at two coronal longitudes different from

TABLE III

Evolution of the energy spectra at different times and positions for the 23 February, 1956 event, which FPR, centered at 23° N 80° W, contains the connecting longitude of 60° W

	Coronal spectra (protons MeV^{-1})					
t_e (UT)/ψ	20° W		60° W		140° W	
	D_0	γ	D_0	γ	D_0	γ
03 : 58			$(1.81 \times 10^{37}$	1.24)[a]		
04 : 01	2.02×10^{34}	3.27				
04 : 14					6.17×10^{35}	0.72
10 : 13			4.9×10^{35}	0.95		
11 : 15			1.3×10^{35}	0.93		
12 : 17			4.8×10^{34}	0.91		

[a] Source spectrum.

that of the connecting one, X_c, the first at the connection point with the flare site (which corresponds to the source spectrum tabulated in Table II) and the other at a point outside of the FPR (110° W). In Table III we illustrate an event when the FPR contains X_c (23 February, 1956) the evolution of the particle spectrum at the coronal position X_c, with several arbitrary times after the ejection of the maximum flux intensity at $\sim$ 03 : 58 UT, when the spectrum was representative of the source spectrum. Also, the evolution of the spectrum at two different longitudinal coronal positions outside of the FPR ($\Psi_f \pm 60°$) is shown.

In Figure 8 the time profiles of the event for three different energies and several longitudinal positions are shown. The profiles show the characteristic diffusive shape outside of the FPR, whereas locations within the FPR show a peculiar decreasing shape.

Figure 9 shows the western asymmetric effect relative to the profile in Figure 8(a). At a distance 50° from the flare on the east side, there are over 100 times fewer particles than at the same distance on the western side. At 60° east, the flux has fallen to negligible levels relative to the western side in Figure 8(a).

In Figure 10 the time regression from the corona back to the top of the FPR is shown. Since regression in time is equivalent to regression in distance from the corona back to the top of the FPR, for a given value of Ψ, any other Ψ', where $\Psi_f < \Psi' < \Psi$, can be seen as a time regression toward the time of particle liberation from the FPR. It must be remembered that time profiles at $\Psi \pm 40°$ begin at $t = 0$. It can be seen in Figures 8–10 that outside the FPR, the onset of particle arrival is delayed proportionally to the distance from the flare site, as indicated by observational profiles in the interplanetary medium.

In Figure 11 azimuthal distributions of the event for several times at three different energies is shown. It can be appreciated that the observational east–west asymmetry

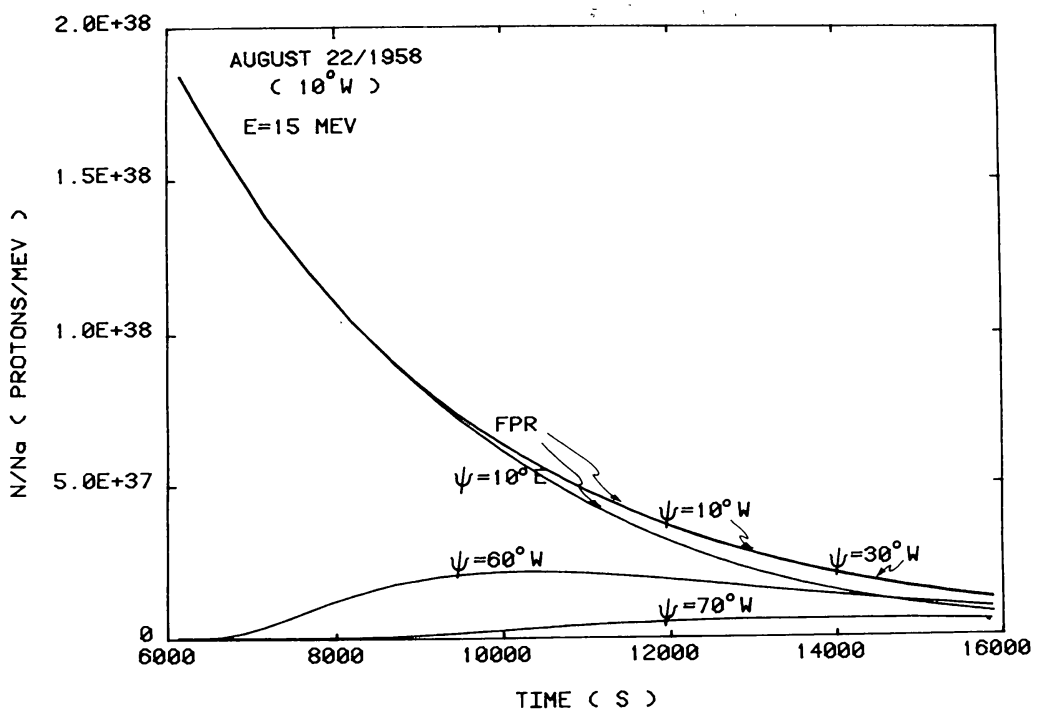

Fig. 8a.

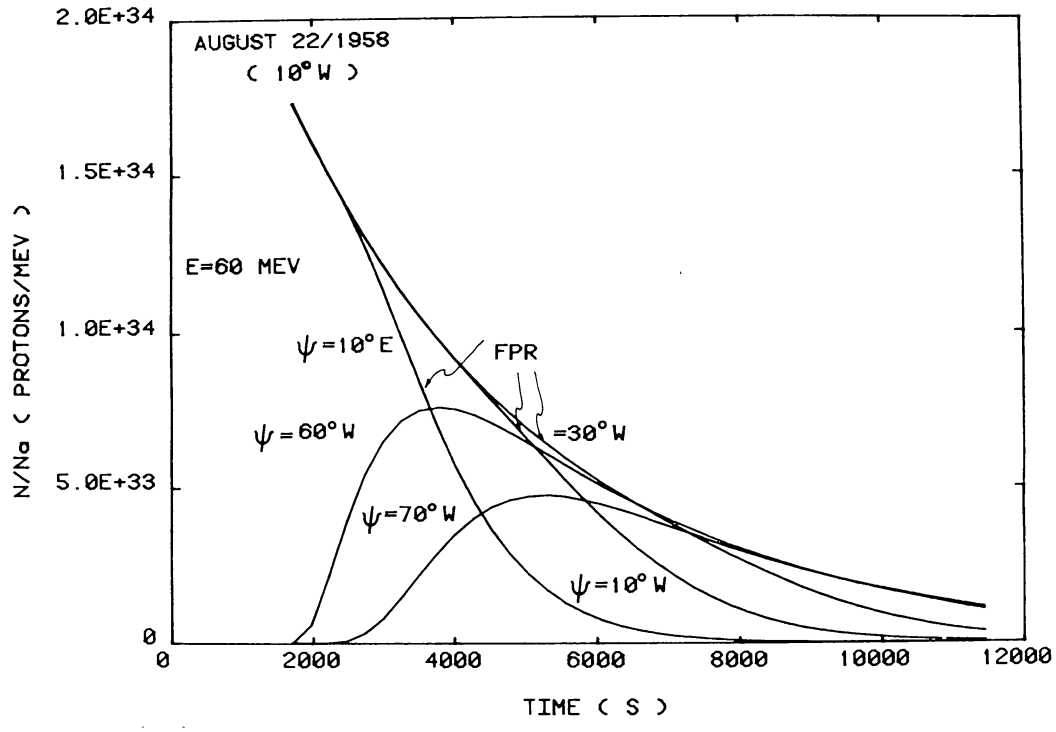

Fig. 8b.

Fig. 8a–c. Coronal time-profile of the 22 August, 1958 event at three different proton energies. Profiles at 60° W and 70° W correspond to particles travelling out of the FPR.

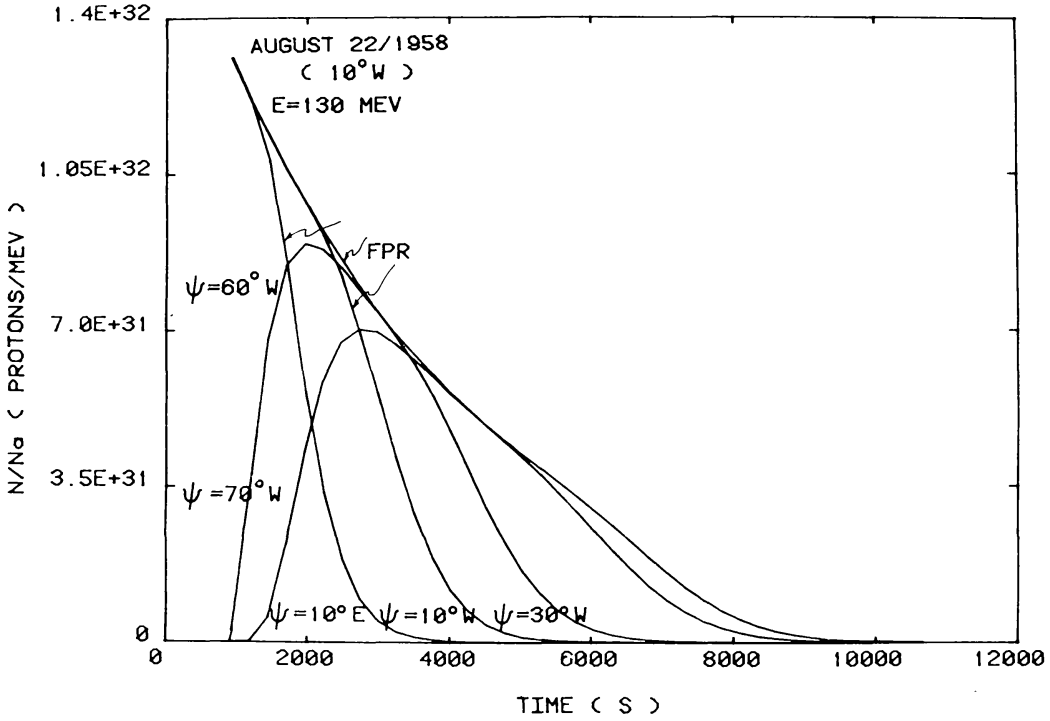

Fig. 8c.

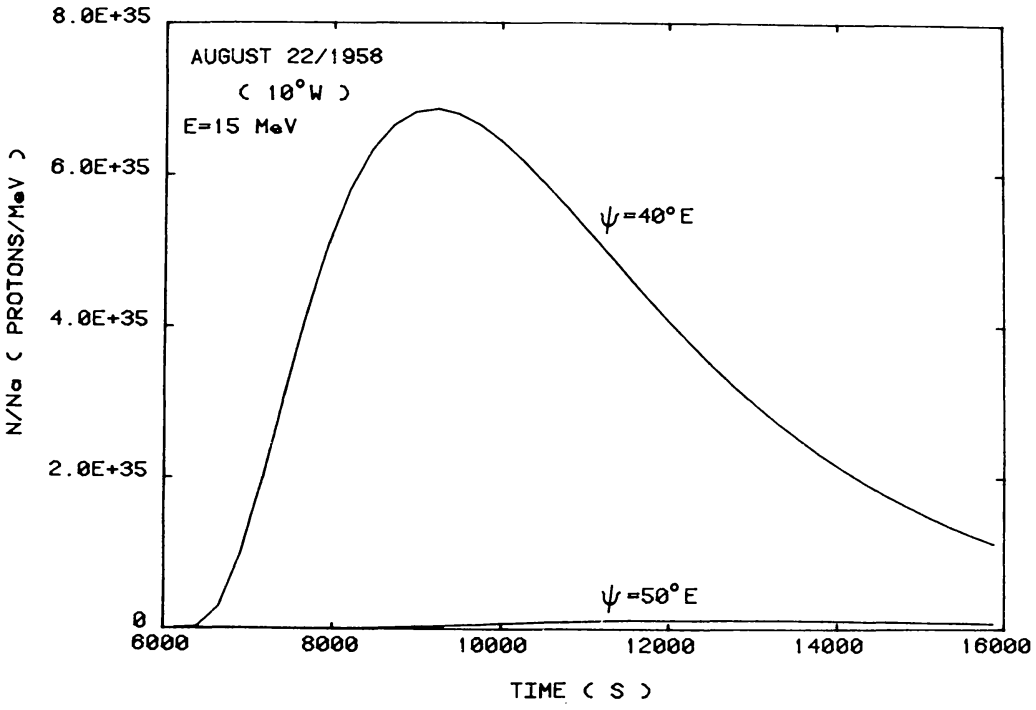

Fig. 9. Time profiles of 15 MeV protons travelling out and East of the FPR, for the 22 August, 1958 event. Comparison with Figure 8(a) shows the east–west asymmetric effect.

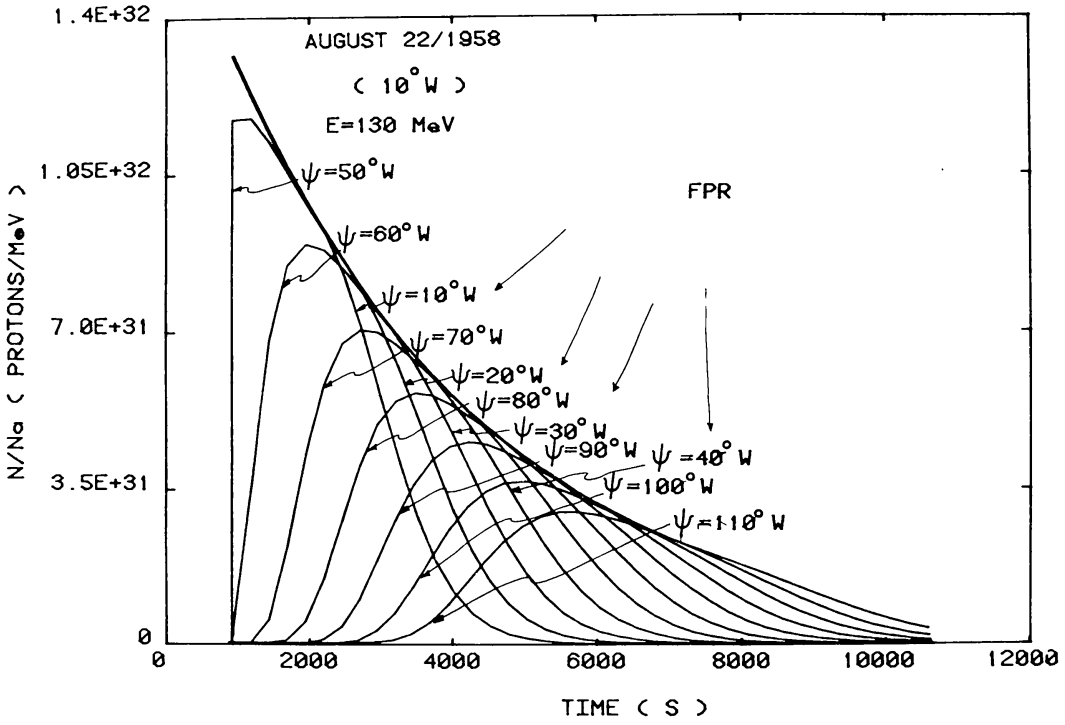

Fig. 10. Regression in time (equivalent to regression in distance from the corona back to the top of the FPR) from 110° W to the edge of the FPR at 50° W.

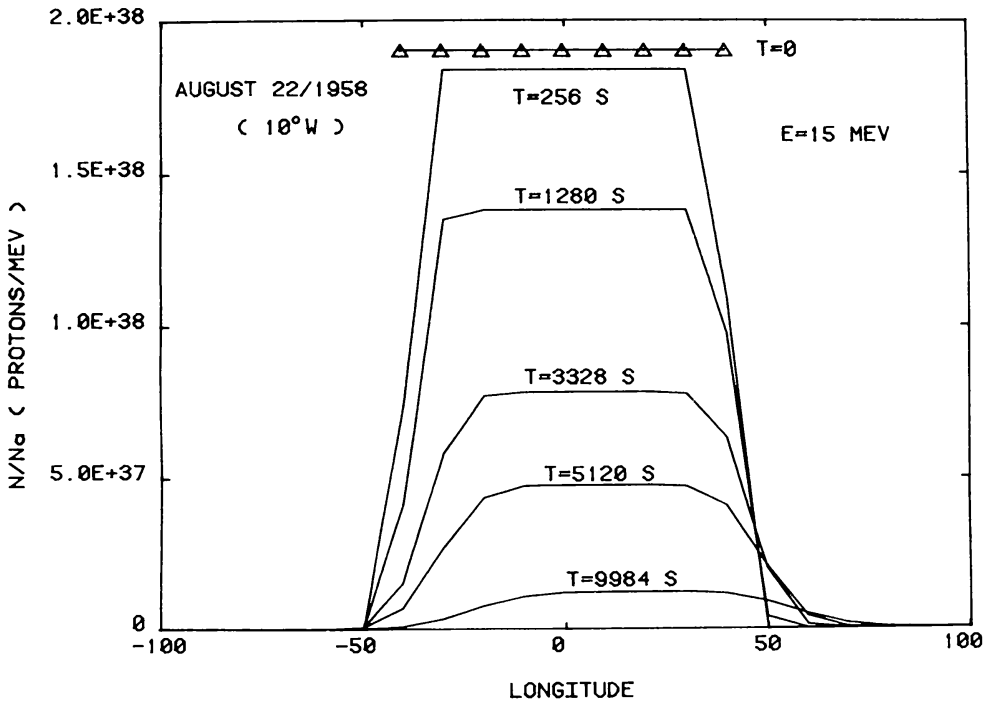

Fig. 11a.

Fig. 11a–c. Azimuthal distributions at three different energies, taking the flare site (10° W) as the origin of longitudinal coordinates since the opening of the FPR up to 2^h46^m of travelling time through the corona.

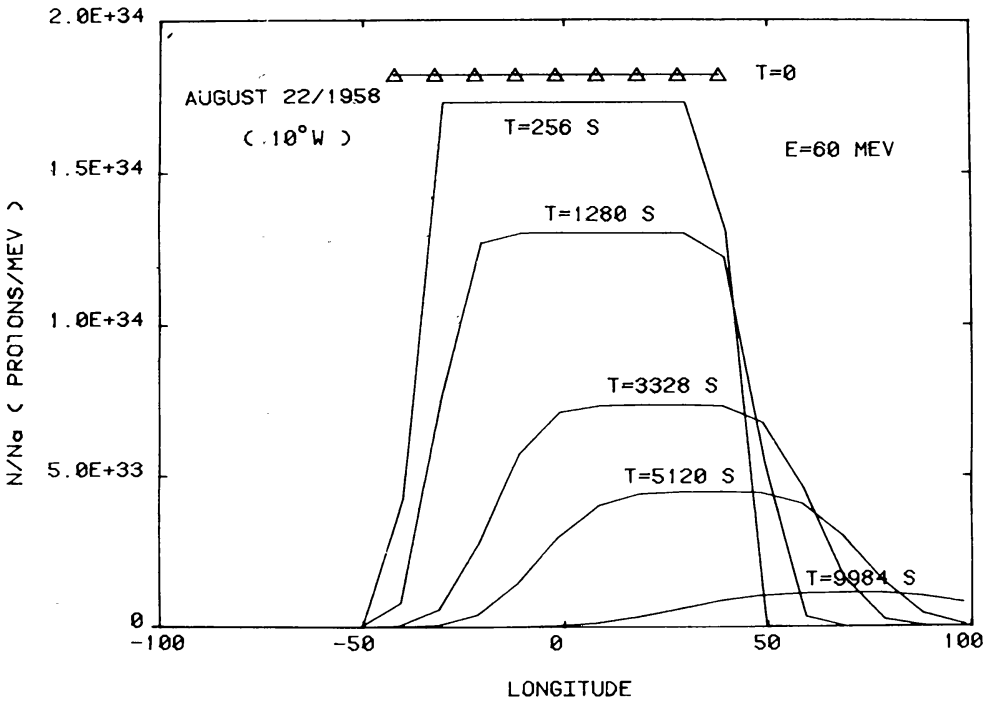

Fig. 11b.

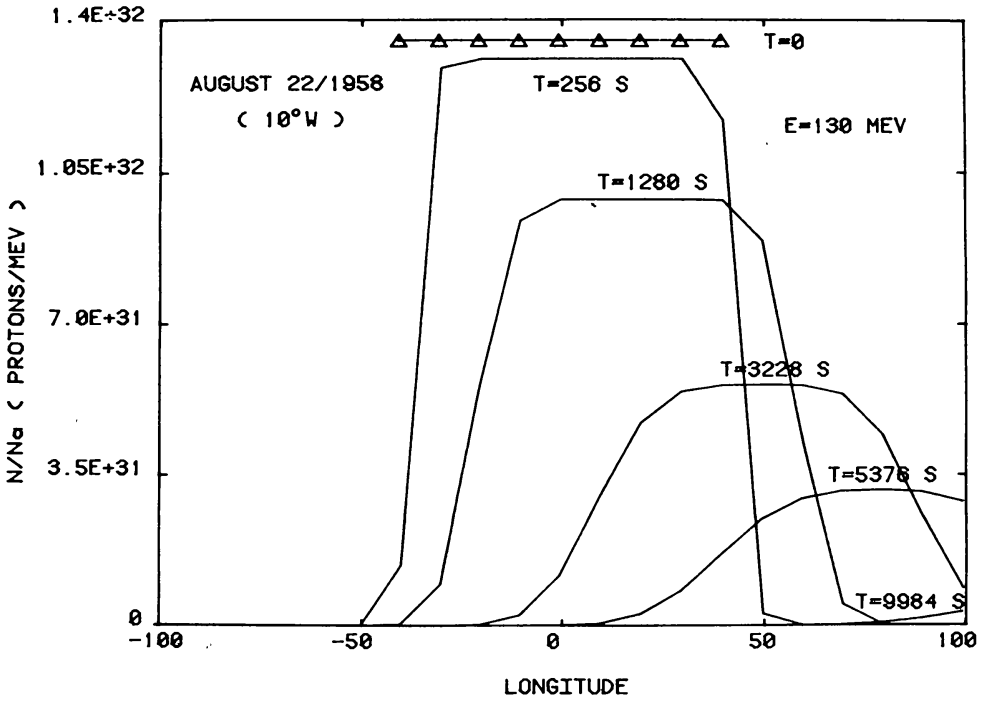

Fig. 11c.

is confirmed by our results. The higher the particle energy, the sharper the effect. Theoretically this is the translation of particle drift in the model.

Though the results displayed in Section 5.2.1 are model dependent, they furnish a clear picture of the evolution of particle energy from the source to the time of particle ejection in interplanetary space. Among the implications of this analysis are our predictions concerning the source energy spectrum and the spectrum at the level of particle ejection into the interplanetary medium. In Table II energy spectra can be seen to flatten at the coronal level, relative to the source spectra in those events where X_c is outside of the FPR, that is, when particles undergo azimuthal propagation to reach point X_c. Also, according to observational features, the wider the separation of the flare site relative to the site of ejection, the longer the transport time of particles to that site. This can be seen from the third and fourth columns of Table II. In events like those of (25 September, 1969), (24 January, 1969) and (28 May, 1972) the travelled distance of particles of the same energy from the edge of the FPR to X_c were 5°, 12° and 50°, respectively. They were covered in 2^h10^m, 2^h21^m, and 3^h12^m, respectively. In contrast, particles in the same energy range of the (1 September, 1971) event took 3^h26^m to cover only 30° distance; when reaching X_c they moved in the west–east direction. Similarly, in the (22 August, 1958) and (29 September, 1968) events, particles of same energy covered 10° and 7° in longitude in 1^h16^m and 59 min, respectively from the edge of the FPR to X_c. In the case of high-energy protons, we can see from the (3 September, 1960 and 28 September, 1961) events, that 108° and 49° were covered in 1^h21^m and 46 min, respectively, while that same distance was covered in the (28 September, 1961) event, by particles of similar energy, in 54 min, travelling in the west–east direction. The derived source energy spectrum for the 22 August, 1958 event is illustrated in Figure 12.

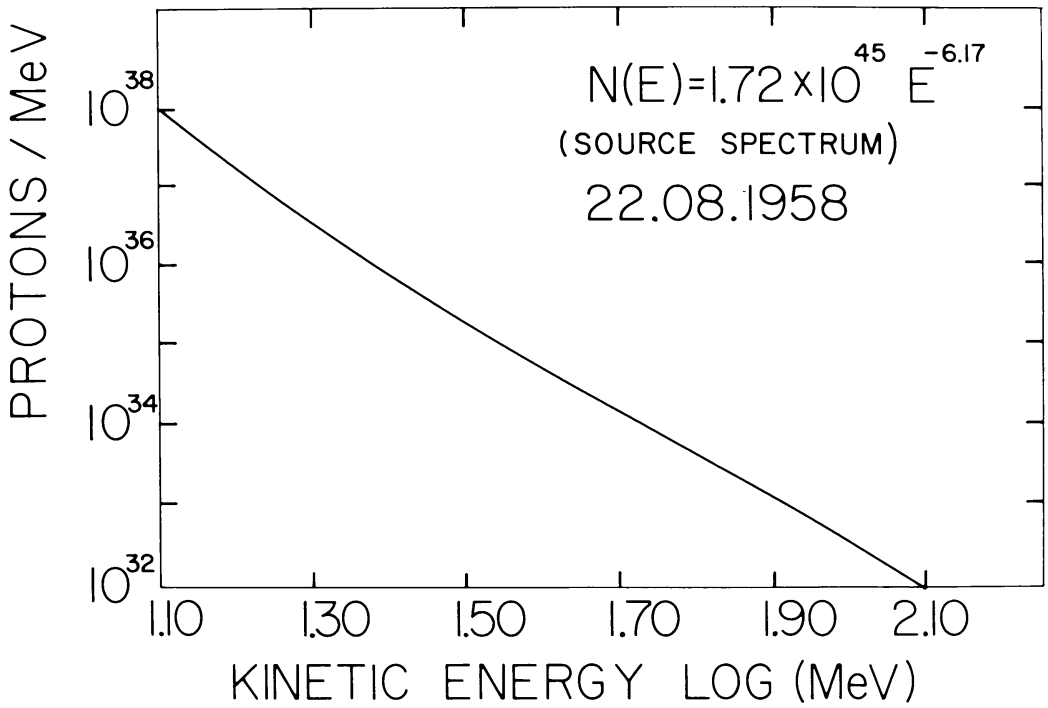

Fig. 12. Source energy spectrum of the 22 August, 1958 event obtained from demodulation of the energy spectrum at the level of the coronal roots of the interplanetary magnetic field lines at 60° W.

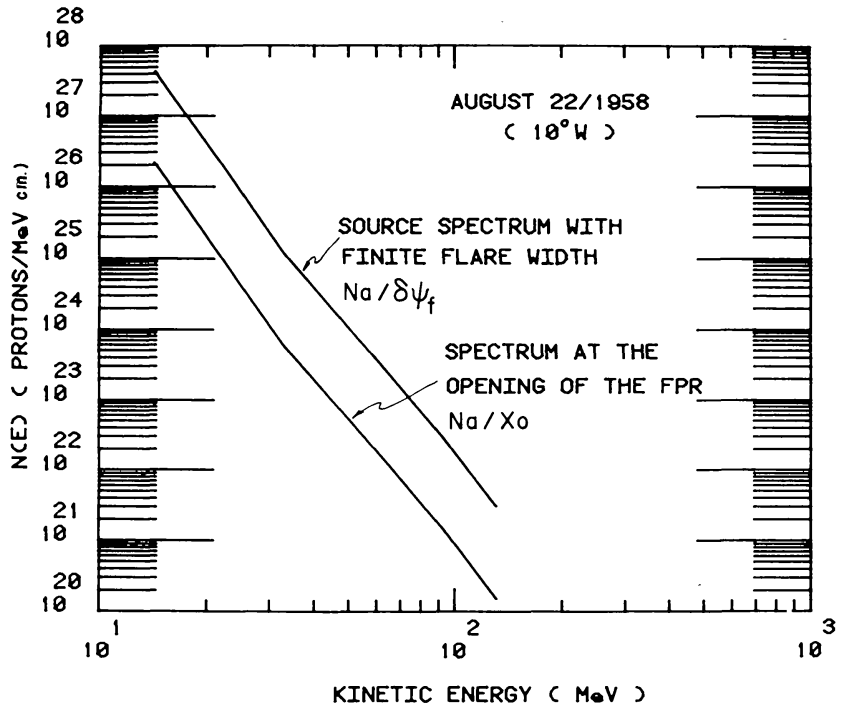

Fig. 13. Source energy spectrum under the assumption of a finite width, $\delta\Psi_f = 8°$, around the flare and spectrum at the opening of the FPR of width $X_0 = 80°$, at the height of 0.9 $R_\odot$ above the photosphere.

In Figure 13 the source spectrum $N_a/\delta\Psi_f$ (protons MeV^{-1} cm^{-1}) is plotted under the assumption of a finite flare width $\delta\Psi = 8°$ together with the spectrum at the top of the FPR at $t = 0$, N_a/X_o (protons MeV^{-1} cm^{-1}). In Figure 14 we have employed Equation

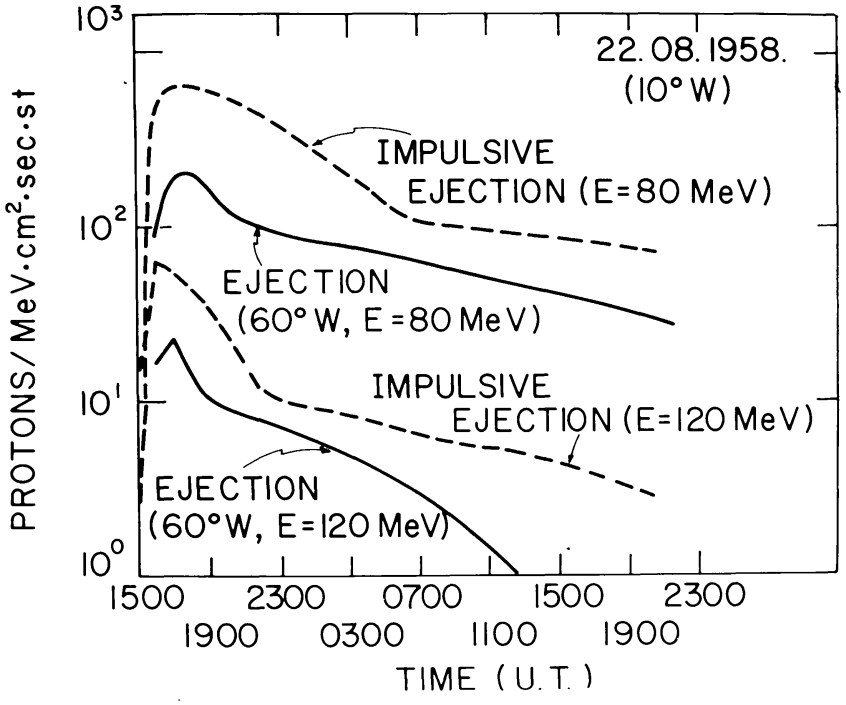

Fig. 14. Predicted time profiles at the Earth's level for two different energies after coronal propagation to reach 60° W, relative to impulsive ejection from the flare site, as if it were not FPR.

(7) to show the effect of coronal propagation in the particle time profile at Earth level in the 22 August, 1958 event, for particles of two different energies, as they would be seen in an interplanetary site connected with the FPR (impulsive ejection), relative to the Earth connected with a solar longitude of 60° W.

In order to test the accuracy of the proposed model, we can proceed in two different forms: first by employing the source energy spectrum of particles derived from neutron and γ-ray line emissions, modulating them for coronal and interplanetary transport to compare with observational data, or second as we did with the events in Table II, by employing interplanetary and coronal demodulation to derive source spectra, and then comparing the results with source spectra derived from electromagnetic radiation. For the task of illustrate this, we have chosen the event of 4 August, 1972. Unfortunately, the observational data is not reliable enough to apply the interplanetary demodulation method of Miroshnichenko (1985) on the basis of the propagation model of Krimigis (1965), because of the overflow of particle intensity in the detectors: therefore, we are limited to using the first alternative.

The first rows of Table IV includes the source energy spectrum of the 4 August, 1972, 9 November, 1979, and 6 November, 1980 events derived from γ-ray line emission. In the next three rows appear the spectra at 60° W and two other longitudes, along with respectives arrival times to those sites as derived from coronal modulation of the source spectra. In Figure 15 time profiles of the 4 August 1972 event are shown for three different energies after interplanetary modulation, in comparison with observational data. These results are model dependent through K_I, v_d, X_0 and the interplanetary diffusion coefficient K is employed in Equations (5) and (7).

TABLE IV

Energy spectra at the coronal level as predicted by modulation of source spectra derived from γ-ray data, and arrival times of the first particles at different coronal longitudes, out of the FPR

Event			$D_0 \bar{E}^{\gamma}$ (protons MeV^{-1})			
			D_0	γ	t_e (UT)	Range (MeV)
4 Aug., 1972	Source (14° N 08° E)		2.03×10^{36}	2.90		10– 80
		68° E	9.72×10^{34}	5.35	07 : 25	
	Coronal	60° W	8.30×10^{32}	1.29	08 : 02	
		82° W	2.84×10^{30}	0.24	08 : 55	
9 Nov., 1979	Source (12° S 02° W)		4.98×10^{35}	3.00		30–100
		58° E	1.64×10^{38}	7.90	03 : 51	
	Coronal	60° W	1.11×10^{33}	1.84	03 : 37	
		92° W	1.19×10^{30}	0.51	04 : 36	
6 Nov., 1980	Source (12° S 74° E)		6.36×10^{34}	2.60		10–100
		134° E	7.66×10^{32}	5.05	04 : 32	
	Coronal	14° E	5.17×10^{32}	1.75	04 : 37	
		60° W	$7.67 \times 10^{27}(-)$	0.33	06 : 07	

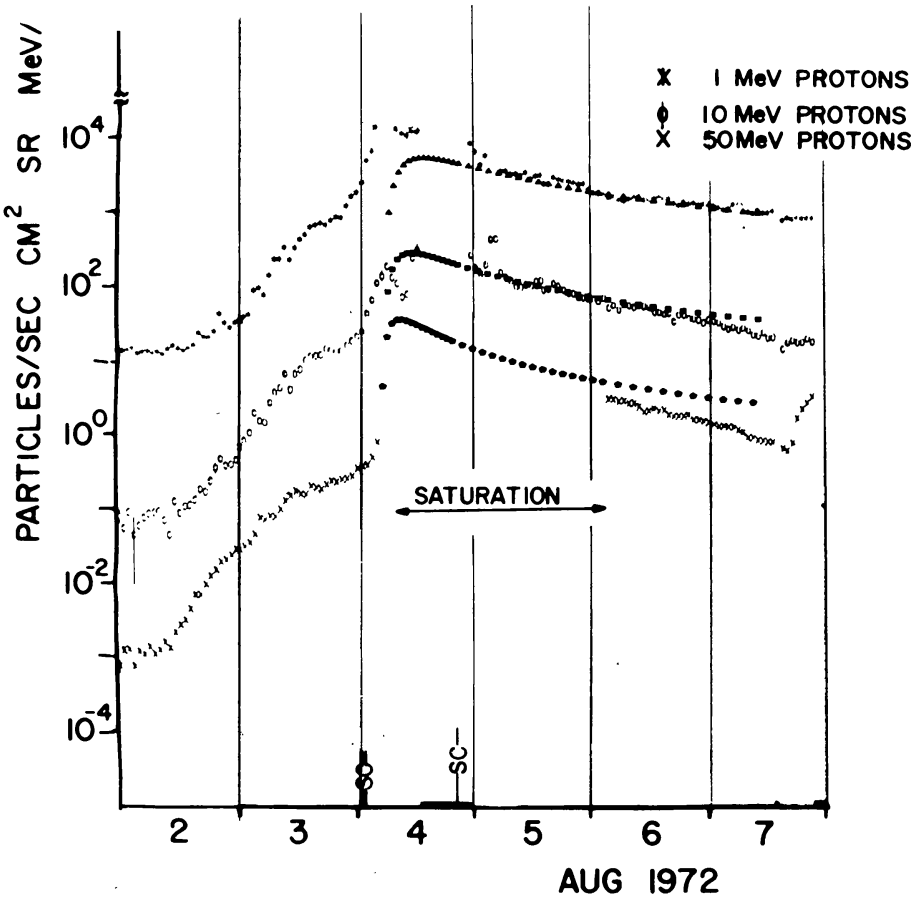

Fig. 15. Predicted time profiles at the Earth's level for three different energies, in comparison with experimental data from the IMPS IV and V. (Data at $E > 20$ MeV is not reliable because of detector saturation.) Interplanetary diffusion coefficient was taken as $K = (15, 2, 3) \times 10^{21}$ cm^2 s^{-1} for protons of 1, 10, and 50 MeV, respectively. Dark squares, triangles, and pentagons are the theoretical curves. Data is from NASA-X-661–74–27 Catalog by M. A. Van Hollebeke, J. R. Wang, and F. B. McDonald.

The predicted results are depressed relative to observational fluxes, so they are multiplied by 100 in Figure 15. We considered that impulsive ejection fluxes would be more consistent with data; however, in that case, that flux would be observed at an interplanetary connection with a solar longitude $\sim 8°$ E but not on the Earth. So, either the model gives a stronger particle depletion at coronal level than the real one, or the employed source spectra has been underestimated. Actually after comparing this with source spectra of similar kinds of events in Table I and II, it seems that the employed data as source spectrum is rather the spectrum after coronal transport from 8° E to 60° W, since its D_0 value is on the same order as those at the coronal level.

Analysis of Tables II and IV indicate that energy spectra of protons to the West of the FPR flatten with azimuthal longitude, because the dominant effect is particle drifts which take preferentially high-energy particles over longer distances. Therefore, the farther the distance, the higher the relative number of high-energy protons to low-energy protons. On the other hand, energy spectra to the east of the FPR become steeper because diffusion is dominant in the east-direction, and so, high-energy particles escape

faster without the balance of drift effects to carry them in a preferential way farther distances.

5.2.2. *Prompt Particle Fluxes*

If we adopt the magnetic bottle model of Schatten and Mullan (1977), we can predict according to the property mentioned at the end of the list in Section 3, the presence of prompt particles before the flare particles can escape from the bottle. As previously mentioned only protons of $E > 100$ MeV may occasionally drift out of the expanding bottle before it is opened and when some restricted conditions are replenished. As was stated by Mullan (1983), the release of the flare population takes between 5–50 min, with a most probable value around $\sim 10^3$ s. Therefore, according to our model, the low-energy proton population (≤ 100 MeV) which is occassionally seen in interplanetary space before the bulk of flare particles, cannot be flare particles. For an explanation of their origin, we propose the following phenomena (Pérez-Peraza and Martinell, 1981): the expanding magnetic bottle finds itself within an active region of a complex magnetic structure, populated with magnetic archs. During its expansion it can get in touch with adjacent field lines of opposite polarity, forming a neutral point that rapidly evolves in a neutral current sheet as the bottle expands (Figure 16). In this sheet, along which there

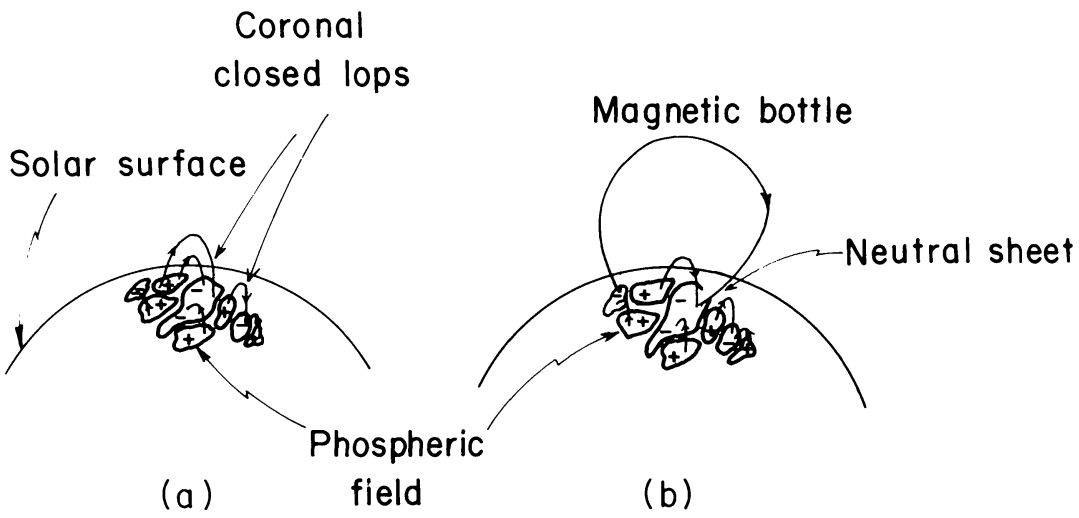

Fig. 16. Expansion of coronal magnetic loops leads to neutral current sheet formation when magnetic archs of opposite polarity get in touch.

is an electric current, a tearing-mode instability may develop due to the fact that though the coronal plasma conductivity is very high, it is not infinite. Magnetic field lines around the neutral sheet are reconnected, transferring their excess energy to local thermal particles. So, according to Furth *et al.* (1963) the grow rate of instability is given as $\omega = (fc^2/4\pi\sigma^2)\,(2s/9\alpha)^{2/5}\ \mathrm{s}^{-1}$, where f takes a value between 0 and 1, $\alpha = ka \sim 0.2$, k is the wave number, a is the width of the neutral current sheet, σ is the coronal conductivity, $s = (4\pi/\rho)^{0.5}\,(\sigma H/c^2)$, with ρ the plasma density, H the field strength and c the light velocity. Taking $H = 3$ G, $\sigma = 10^{16}\ \mathrm{s}^{-1}$ and $\rho = 1.6 \times 10^{-16}\ \mathrm{g\ cm}^{-3}$ as typical coronal values below $\sim 1\,R_\odot$, the growth rate becomes

$\omega = 2.77 \times 10^5\, a^{-8/5}\ \mathrm{s}^{-1}$. Now, assuming an expansion velocity in the form $V_c = V_0 \exp(-t/t_e)$ the current sheet width decreases as $a = d \exp(-t/t_e)$ where d is the initial width of the sheet, $t_e = d/V_0$ is the exponential compression time and V_0 is the bottle velocity when the archs join. For calculations, we make the following assumptions: since a certain time interval has elapsed when the expanding bottle finds a magnetic loop of opposite polarity, the velocity V_0 must be lower than the initial expansion velocity; if we take $V_0 = 1000\ \mathrm{km\ s}^{-1}$ in Figure 17, we can see the plotted

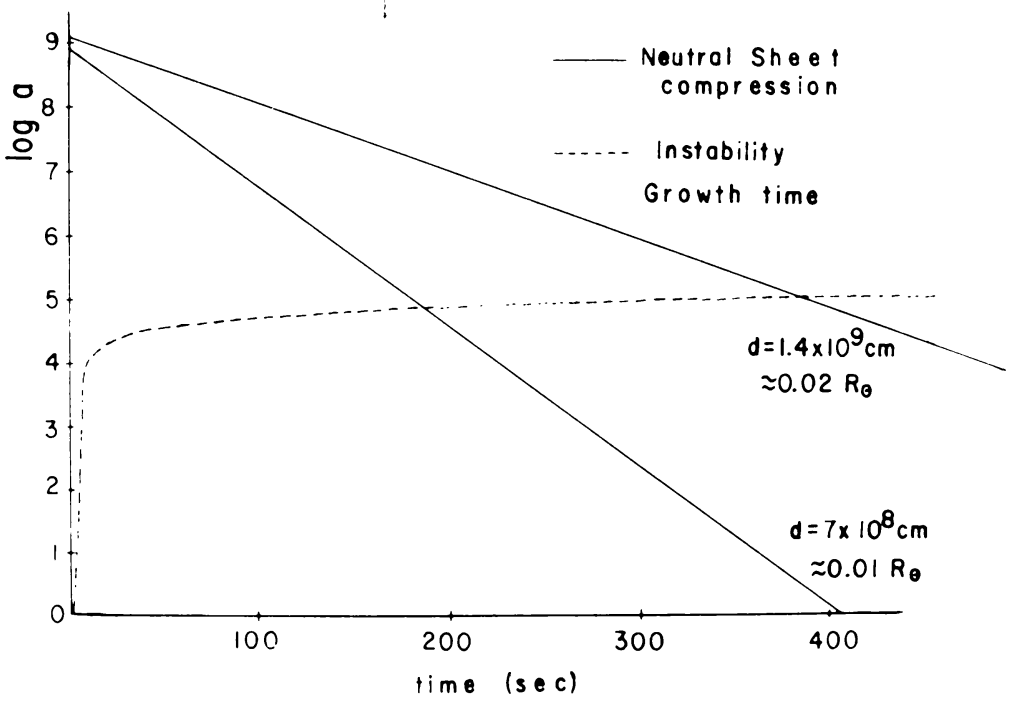

Fig. 17. Grow time for the tearing-mode instability versus the evolution of the current sheet width, which is being compressed from an initial width d.

growth time for the instability ω^{-1} versus the evolution of the width a for two reasonable values of the initial sheet width d, 0.01 $R_\odot$ and 0.02 $R_\odot$. The intersection of each of these curves gives the growth time and the width of the neutral sheet corresponding to those times. It can be seen that these become, $t = 31.5$ s with $a = 2.19 \times 10^4$ cm and $t = 64.5$ s with $a = 3.41 \times 10^4$ cm for the specific initial conditions, respectively. To these times, we need to add the time elapsed since the expansion of the bottle till the formation of the neutral sheet. As we said before, the magnetic loops that may interact with the expanding bottle must be found in the same active region. Consequently, their distances from the magnetic bottle cannot be larger than the dimensions of the active regions, which are typically on the order of 0.1 $R_\odot$. Thus, the time that the bottle needs to reach a magnetic arch, if the initial expansion velocity is $\sim 1200\ \mathrm{km\ s}^{-1}$, is at the most $t = 0.1\, R_\odot / 1200\ \mathrm{km\ s}^{-1} = 1$ min. Therefore, we conclude that a particle population may be accelerated out of the flare site after 1.5–2 min of the initial magnetic bottle expansion. This is clearly less time than liberation time from the bottle 5–50 min.

The electric field produced by the change of the magnetic field structure around the neutral layer appears from the Faraday law as $\varepsilon = \omega HL/c$, where L is the length scale

of the electric field and ω^{-1} is the time of the magnetic field structure change, considered as the grow time for the instability. Taking the length of the neutral sheet of 0.05 $R_\odot$, and since the electric field appears in a direction parallel to the neutral sheet, we can consider this length as the scale L. Therefore, for a magnetic field $H = 1$ G around the neutral sheet, we have $\varepsilon = 3.7 \times 10^{-3}$ statvolt cm^{-1} for $\omega^{-1} = 31.5$ s and $\varepsilon = 1.8 \times 10^{-3}$ statvolt cm^{-1} for $\omega^{-1} = 64.5$ s. The energy obtained from this magnetic energy dissipation process in the volume L^2a of the neutral sheet is 1.46×10^{17} erg and in 5.38×10^{16} erg, respectively. Clearly, this liberated energy is at least 10^{13} times lower than the energy liberated in the flare, but is enough to produce a bunch of particles with energies as high as $\mathbf{E}_{max} = e\varepsilon L = 3.7$ GeV and 1.81 GeV, respectively. Some of these accelerated particles are impulsively ejected, while others may undergo azimuthal propagation.

It should be remembered that we have referred to three different emission phases within the frame of this model: the impulsive phase of primary flare particles, the emission of stochastically accelerated particles, and the emission of prompt particles out of the flare magnetic bottle. We should mention, according to Mullan (1983), an additional particle emission up in the corona coming from acceleration in the reconnection processes during the bottle opening, giving rise to relativistic electrons.

5.3. Summary

We will end this section with an analytical criticism of the proposed model; by evoking the dynamical behavior of the flare magnetized plasme, property (d) can be explained by an FPR where particles are convected at the expansion rate of the magnetic structure, with an average velocity that may vary from event to event. For instance, if the average expansion velocity is of 10^3 km s^{-1} and opens at 1 $R_\odot$ above the solar surface, the rate is $\sim <150°/h>$, whereas if $V_c = 350$ km s^{-1}, and opens at 0.8 $R_\odot$, the transport rate is $\sim <60°/h>$. In this way property (e) satisfies velocity and energy independence of low energy particles, while high-energy particles drift from the confining structure with a velocity-dependent rate. Particle transport of low-energy particles out of the FPR is dominated by a diffusive thick geometry, introducing a slight velocity-dependence, while high-energy particle behavior is energy-dependent through a drift-type transport. The strong anisotropy observed in some events during the initial phase of events is explained by the impulsive ejection of particles during a first emission phase taking place during the flare impulsive phase. This also allows us to explain the arrival of low-energy electrons before protons of the same energy, because the latter have a lower velocity, and eventually they mix with those from the secondary acceleration stage, which are liberated several minutes later. On the other hand, the location of maximum peak intensity in many events over the flare site is also a consequence of the impulsive emission phase. An absence of this first emission phase allows for an occasional shift of the maximum peak intensity to other preferential liberation regions, and the observation of a wide cone of anisotropy at the beginning of the event, instead of a narrow cone, as in the previously mentioned case. An increase of the slope with azimuthal distance in the initial phase of some particle events or its constancy in other events depends on

whether the first emission phase takes place or not. The characteristic change of slope in particle energy spectra (around 100 keV for electrons) indicates the occurrence of the first and second emission of solar flare particles. The spectral slope decrease in longitude during the decay phase of events is attributed to preferential drift of high-energy particles relative to low-energy particles. Property (f) concerning the modulation of particle fluxes when they travel from one unipolar sector to another of opposite polarity is only described qualitatively in terms of fluctuations of κ_l and v_d, when particles find quasi-equilibrium neutral sheets (a very low rate of field line diffusion) that do not generate intense accelerating electric fields, but rather act as particle propagation modulators. In order to quantify this effect, some reliable perturbations on the two propagation parameters should be included in the calculations, i.e., the drift velocity and the diffusion coefficient.

Observational features (a), (b), (c), and (g) have been quantitatively reproduced by means of transport equations within the frame of the model. The eventual presence of prompt protons of all energies before the bulk of flare particles has been quantitatively predicted by an additional emission phase in a compressed coronal neutral sheet. Relativistic electrons associated with type-IV bursts may appear in the reconnection processes during the bottle opening (Mullan, 1983).

6. Conclusions

Perspectives for deeply understanding solar particle azimuthal transport are undoubtedly associated with future multi-spacecraft observations, making possible a fine structure in the temporal and spatial behavior of particle fluxes, azimuthal and radial effects for different solar ions and electrons, simultaneously with other flare emissions and measurement of magnetic fields, solar wind and local physical parameters. This will allow for greater discrimination between particle coronal propagation and escape effects from the coronal magnetic fields. In particular, the 'out of the ecliptic' space probe experiments will bring new light to coronal transport of flare particles. From the theoretical point of view, it is interesting to search for specific functions of the escape rate, $\Gamma(\Psi)$, which allows, for a better description of the preferential liberation at some definite longitudes and escape inhibition at other longitudes, since a plausible time and velocity dependence of the escape process has not yet been established. This may be carried out in principle, by new detailed numerical calculations of particle trajectories in a suitable coronal magnetic field topology. This, however, requires further information about the behavior and evolution of magnetic fields in the course of a solar event. Very outstanding advances may be expected in the determination of the complete coronal vector magnetic field with the simultaneous application of the Hanle effect for two emission lines, which makes it possible to determine in an unambiguous manner the three components of the field (e.g., Bommier *et al.*, 1981).

Finally, it should be mentioned that despite the fallacies of the proposed model in confrontation with specific solar particle events, the main goal of this proposal is to emphasize the importance of the particle multi-emission phase character of the flare

phenomenon, although the number of phases and their relative importance may vary from event to event.

Acknowledgements

I sincerely thank the Local Organizing Committee of the 9th ECRS, particularly Profs. E. Fischer and K. Kudela, for their kind reception and assistance in Kŏsice, where this talk was presented as an Invited Lecture. I also thank the Dirección General de Investifación Científica y Superación Académica, S.E.S.I.C. of the S.E.P. and CONACYT for financial support allowing me to attend this Conference.

References

Allum, F. R., Palmeira, R. A. R., Rao, U. R., McCracken, K. G., Harries, J. F., and Palmer, L.: 1971, *Solar Phys.* **17**, 241.
Amata, E. V., Domingo, V., Page, D. E., and Wenzel, K. P.: 1975, *Proc. 14th Int. Cosmic Ray Conf.* **5**, 1761.
Anderson, K. A. and Lin, R. P.: 1966, *Phys. Rev. Letters* **16**, 1121.
Axford, W. I.: 1965, *Planetary Space Sci.* **13**, 1301.
Barouch, E., Gros, M., and Masse, P.: 1971 *Solar Phys.* **19**, 483.
Bazilevskaya, G. A. and Vashenyuk, E. V.: 1979, *Proc. 16th Int. Cosmic Ray Conf.* **5**, 156.
Bazilevskaya, G. A. and Vashenyuk, E. V.: 1981, *Proc. 17th Int. Cosmic Ray Conf.* **3**, 93.
Belovskii, M. N. and Ochelkov, Yu. P.: 1980, *Astron. J.* **57**, 119.
Benz, A. O. and Gold, T.: 1971, *Solar Phys.* **21**, 157.
Bomier, V., Leroy, J. L., and Sahal-Brechot, S.: 1981, *Astron. Astrophys.* **100**, 231.
Bryant, D. A., Cline, T. L., Desai, V. D., and McDonald, F. B.: 1962, *J. Geophys. Res.* **67**, 4983.
Bukata, R. P., Rao, V. R., McCracken, K. G., and Keath, E. P.: 1972, *Solar Phys.* **26**, 229.
Burlaga, L. F.: 1970, *Acta Phys. Acad. Sci. Hungaricae* **29**, Suppl. 2, 9.
Chup, E. L. and Forrest, D. F.: 1982, Invited talk AAS Meeting, *High Energy Neutral Radiations from Solar Flares*, Boulder, Col.
Cliver, E. W., Kahler, S. W., Shea, M. A., and Smart, D. F.: 1982, *Astrophys. J.* **260**, 362.
Coleman, P. J., Jr.: 1966, *J. Geophys. Res.* **71**, 5509.
Conlon, T. F., McDonald, F. B., Van Hollebeke, M. A. I., and Trainor, J. H.: 1979, *Proc. 16th Int. Cosmic Ray Conf.* **5**, 152.
Datlowe, D.: 1972, *J. Geophys. Res.* **77**, 5374.
Duggal, S. P.: 1975, *Rev. Geophys. Space Phys.* **13**, 1084.
Duggal, S. P. and Pomerants, M. A.: 1973, *J. Geophys. Res.* **78**, 7205.
Duggal, S. P., Guidi, I., and Pomerants, M. A.: 1971, *Solar Phys.* **19**, 234.
Englade, R. C.: 1971, *J. Geophys. Res.* **76**, 6190.
Fan, C. Y., Pick, M., Pyle, R., Simpson, J. A., and Smith, D. R.: 1968, *J. Geophys. Res.* **73**, 1555.
Feit, J.: 1973, *Solar Phys.* **29**, 211.
Fisk, L. A. and Schatten, K. H.: 1972, *Solar Phys.* **23**, 204.
Furth, H. P., Killeen, J., and Rosenbluth, M. N.: 1963, *Phys. Fluids* **6**, 459.
Gold, R. E. and Roelof, E. C.: 1979, *Proc. 16th Int. Cosmic Ray Conf.* **5**, 46.
Gold, R. E., Notle, J. T., Roelof, E. C., and Reinhard, R.; 1973, *Proc. 13th Int. Cosmic Ray Conf.* **2**, 1367.
Gold, R. E., Krimigis, S. M., Roelof, E. C., Krieger, A. S., and Nolte, J. T.: 1975, *Proc. 14th Int. Cosmic Ray Conf.* **5**, 1710.
Gold, R. E., Keath, E. P., Roelof, E. C., and Reinhard, R.: 1977, *Proc. 15th Int. Cosmic Ray Conf.* **5**,125.
Gombosi, T., Kecskemety, K., Merenyi, E., Tátrallyay, M., Kurt, V. G., Logachev, Yu. I., Stolpovskii, V. G., and Trebukhocskaya, G. A.: 1979, *Proc. 16th Int. Cosmic Ray Conf.* **5**, 163.
Gombosi, T., Kóta, J., Somogyi, A. J., Kurt, V. G., Kuzhevskii, B. M., and Logachev, Yu. I.: 1977, *Solar Phys.* **54**, 441.
Helios/IMP/Voyager Workshop study Group: 1979, *Proc. 16th Int. Cosmic Ray Conf.* **5**, 151.
Hudson, H. S.: 1978, *Solar Phys.* **54**, 237.

Jopikii, J. R. and Parker, E. N.: 1969, *Astrophys. J.* **155**, 799.
Keath, E. P., Bukata, R. P., McCracken, K. G., and Rao, U. R.: 1971, *Solar Phys.* **18**, 503.
Kecskemety, K., Gombosi, T. I., Somogyi, A. J., Szentgali, A., Wibberenz, G., Green, G., Kunow, H., Steffens, V., Durt, V., Logachev, Yu. I., Pissarenko, N. F., and Stolpovsky, V. G.: 1981, *Proc. 17th Int. Cosmic Ray Conf.* **3**, 89.
Kennel, C. F. and Petschek, H. E.: 1966, *J. Geophys. Res.* **71**, 1.
Krimigis, S. M.: 1965, *J. Geophys. Res.* **70**, 2943.
Krimigis, S. M.: 1973, in *Solar Terrestrial Relations Conference*, Calgary, 277.
Krimigis, S. M., Roelof, E. C., Armstrong, T. P., and Van Allen, J. A.: 1971, *J. Geophys. Res.* **76**, 5921.
Kunow, H., Green, G., Muller-Mellin, R., Wibberenza, G., Tátrallyay, M., Gombosi, T. I., Kecskemety, K., Kurt, V., Logachev, Yu. I., and Stolporsky, V. G.: 1981, *Proc. 17th Int. Cosmic Ray Conf.* **3**, 88.
Kunow, H., Wibberenz, G., Green, G., Muller-Mellin, R., Witte, M., Hempe, H., and Fuckner, J.: 1977, *Contributed Papers to the Study of Travelling Interplanetary Phenomena*, Tel Aviv, COSPAR Symp., AFGL-TR-770309, pp. 363.
Lanzerotti, J. L.: 1973, *J. Geophys. Res.* **78**, 3942.
Lin, R. P.: 1970, *Solar Phys.* **12**, 266; **15**, 453.
Lockwood, J. A. and Debrunner, H.: 1983, *Proc. 18th Int. Cosmic Ray Conf.* **4**, 185.
Lockwood, J. A. and Debrunner, H.: 1984, Preprint of Contribution SH-6 in the 9th European Cosmic Ray Simposium, Konsice.
Lüst, R. and Simpson, J. A.: 1957, *Phys. Rev.* **108**, 1563.
Martinell, J. and Pérez-Peraza, J.: 1981, *Rev. Mexicana Astron. Astrof.***6**, 350.
Ma Sung, L. S.: 1977, Ph.D. Thesis, University of Maryland, NASA X-660–77–113.
Ma Sung, L. S. and Earl, J. A.: 1978, *Astrophys. J.* **222**, 1080.
Ma Sung, L. S., Van Hollebeke, M. A. I., and McDonald, F. B.: 1975, *Proc. 14th Int. Cosmic Ray Conf.* **5**, 1762.
McCracken, K. G., Rao, U. R., and Bukata, R. P.: 1967, *J. Geophys. Res.* **72**, 4293.
McCracken, K. G. and Rao, U. R.: 1970, *Space Sci. Rev.* **11**, 155.
McCracken, K. G., Rao, U. R., Bukata, R. P., and Keath, E. P.: 1971, *Solar Phys.* **18**, 100.
McDonald, F. B. and Dessai, U. D.: 1971, *J. Geophys. Res.* **76**, 808.
McGuire, R. E., Van Hollebeke, M. A. I., and Lal, N.: 1983a, *Proc. 18th Int. Cosmic Ray Conf.* **10**, 353.
McGuire, R. E., Lal, N., and Van Hollebeke, M. A. I.: 1983b, *Proc. 18th Int. Cosmic Ray Conf.* **10**, 357.
McIntosh, P. S.: 1972, *Rev. Geophys. Space Phys.* **10**, 837.
McKibben, R. B.: 1972, *J. Geophys. Res.* **77**, 3957.
McKibben, R. B.: 1973, *J. Geophys. Res.* **78**, 7184.
Meersons, B. I. and Sasorov, P. V.: 1981, *Adv. Space Res.* **1**, 77.
Meersons, B. I. and Rogachevskii, I. V.: 1983, *Solar Phys.* **87**, 337.
Miroshnichenko, L. I.: 1985, *IZMIRAN Preprints* **15** 548.
Miroshnichenko, L. I. and Petrov, B. M.: 1985, *Dynamics of Radiations Conditions in Space*, Energoatmizdat, Moscow.
Mullan, D. J.: 1976, *Astron. Astrophys.* **52**, 305.
Mullan, D. J. and Schatten, K. H.: 1979, *Solar Phys.* **62**, 153.
Mullan, D. J.: 1983, *Astrophys. J.* **269**, 765.
Newkirk, G., Jr.: 1973, NASA Special Publ. No. 343, p. 453.
Newkirk, G., Jr. and Wentzel, D. G.: 1978, *J. Geophys. Res.* **83**, 2009.
Ng, C. K. and Gleeson, L. J.: 1976, *Solar Phys.* **46**, 347.
Notle, J. T. and Roelof, E. C.: 1973, *Solar Phys.* **33**, 241.
O'Gallagher, J. J. and Simpson, J. A.: 1966, *Phys. Rev. Letters* **16**, 1212.
Owens, A. J.: 1979, *J. Geophys. Res.* **84**, 4451.
Parker, E. N.: 1963, *Interplanetary Dynamic Processes*, Interscience, Wiley and Sons, New York.
Parker, E. N. and Stewart, H. A.: 1967, *J. Geophys. Res.* **72**, 5287.
Pérez-Peraza, J.: 1975, *J. Geophys. Res.* **80**, 3535.
Pérez-Peraza, J., Gálvez, M., and Lara, R.: 1977, *Proc. 15th Int. Cosmic Ray Conf.* **5**, 23.
Pérez-Peraza, J. and Gálvez, M.: 1978, *Space Research* **XVIII**, 365.
Pérez-Peraza, J. and Martinell, J.: 1981, *Proc. 17th Int. Cosmic Ray Conf.* **3**, 55.
Pérez-Peraza, J., Alvarez-Madrigal, M., Rivero, F., and Miroshnichenko, L. I.: 1985, *Proc. 19th Int. Cosmic Ray Conf.* **4**, 110.

Perron, C., Domingo, V., Reinhard, R., and Wenzel, K. P.: 1978, *J. Geophys. Res.* **83**, 2017.
Priest, E. R.: 1981, *Solar Flare Magnetohydrodynamics* Gordon Breach Publ., New York, p. 2.
Rao, U. R., McCracken, K. G., Allum, F. R., Palmeira, R. A. R., Bartley, W. C., and Palmer, I.: 1971, *Solar Phys.* **19**, 209.
Reid, G.: 1964, *J. Geophys. Res.* **69**, 2659.
Reinhard, R. and Roelof, E. C.: 1973, *Proc. 13th Int. Cosmic Ray Conf.* **2**, 1378.
Reinhard, R. and Wibberenz, G.: 1973, *Proc. 13th Int. Cosmic Ray Conf.* **2**, 1372.
Reinhard, R. and Wibberenz, G.: 1974, *Solar Phys.* **36**, 473.
Reinhard, R.: 1975, *Proc. 14th Int. Cosmic Ray Conf.* **5**, 1687.
Reinhard, R., Domingo, V., Perron, C., and Wenzel, K. P.: 1977, *Proc. 15th Int. Cosmic Ray Conf.* **5**, 107.
Roelof, E. C.: 1973, *Proc. Solar-Terrestrial Relations Conference*, Calgary.
Roelof, E. C. and Krimigis, S. M.: 1973, *J. Geophys. Res.* **78**, 5375.
Roelof, E. C., Gold, R. E., Krimigis, S. M., Krieger, A. S., Notle, J. T., McIntosh, P. S., Lazarus, A. J., and Sullivan, J. D.: 1975, *Proc. 14th Int. Cosmic Ray Conf.* **5**, 1704, 1692.
Sakurai, K.: 1965, *Rep. Ionos. Space Res. Japan* **19**, 408.
Sakurai, K.: 1971, NASA Report X-693–71–268 GSFC, Greenbelt Md.
Sakurai, K.: 1973, *Solar Phys.* **31**, 483.
Schatten, K. H.: 1970, *Solar Phys.* **12**, 484.
Schatten, K. H. and Mullan, D. J.: 1977, *J. Geophys. Res.* **82**, 5609.
Schulze, B. M., Ritcher, A. K., and Wibberenz, G.: 1977, *Solar Phys.* **54**, 207.
Sekido, Y. and Murakami, K.: 1955, *Proc. 5th Int. Cosmic Ray Conf.* **000**, 253.
Simnett, G. M.: *Solar Phys.* **20**, 448.
Simnett, G. M.: 1972, *Solar Phys.* **22**, 189.
Simnett, G. M. and Holt, S. S.: 1971, *Solar Phys.* **16**, 208.
Svalgard, L., Wilcox, J. M., and Duvall, T. L.: 1974, *Solar Phys.* **37**, 157.
Van Hollebeke, M. A. I., Ma Sung, L. S., and McDonald, F. B.: 1975, *Solar Phys.* **41**, 189.
Vashenyuk, E. V., Bazilevskaya, G. A., and Charakchyan, T. N.: 1977, *Proc. 15th Int. Cosmic Ray Conf.* **5**, 148.
Wang, J. R.: 1972, NASA-661–72–761, GSFC.
Wibberenz, G. and Reinhard, R.: 1975, *Proc. 14th Int. Cosmic Ray Conf.* **5**, 1681.
Zel'dovich, M. A., Kuzhevsky, B. M., Logachev, Yu. I.: 1977, *Proc. 15th Int. Cosmic Ray Conf.* **5**, 198.